*J. Fluid Mech.* (2006), *vol.* 557, *pp.* 369–397.  
doi:10.1017/S0022112006009815 Printed in the United Kingdom

# Third-order theory for bichromatic bi-directional water waves

By PER A. MADSEN AND DAVID R. FUHRMAN

Department of Mechanical Engineering, Technical University of Denmark, 2800 Kgs Lyngby, Denmark

(Received 3 October 2005 and in revised form 21 November 2005)

A new third-order solution for bichromatic bi-directional water waves in finite depth is presented. Earlier derivations of steady bichromatic wave theories have been restricted to second-order in finite depth and third-order in infinite depth, while third-order theories in finite depth have been limited to the case of monochromatic short-crested waves. This work generalizes these earlier works. The solution includes explicit expressions for the surface elevation, the amplitude dispersion and the vertical variation of the velocity potential, and it incorporates the effect of an ambient current with the option of specifying zero net volume flux. The nonlinear dispersion relation is generalized to account for many interacting wave components with different frequencies and amplitudes, and it is verified against classical expressions from the literature. Limitations and problems with these classical expressions are identified. Next, third-order resonance curves for finite-amplitude carrier waves and their three-dimensional perturbations are calculated. The influence of nonlinearity on these curves is demonstrated and a comparison is made with the location of dominant class I and class II wave instabilities determined by classical stability analyses. Finally, third-order resonance curves for the interaction of nonlinear waves and an undular sea bottom are calculated. On the basis of these curves, the previously observed downshift/upshift of reflected/transmitted class III Bragg scatter is, for the first time, explained.

## 1. Introduction

Monochromatic short-crested water waves occur in connection with, for example, oblique reflection from seawalls and diffraction around detached breakwaters. As a first linear approximation, they can be obtained by the superposition of two oblique travelling wavetrains of equal frequency and amplitude. A second-order solution was derived by Fuchs (1952), whereas Chappelear (1961) extended it to third-order. Hsu, Tsuchiya & Silvester (1979) rederived the third-order solution with a different choice of expansion parameter. Since then the literature on this subject has been extensive and we shall only mention a few of the important contributions: Roberts (1983) developed a high-order perturbation method for short-crested deep-water waves, while Roberts & Peregrine (1983) treated the important limit of grazing angles, where the short-crested deep-water waves become long-crested. Numerical computations of highly nonlinear short-crested waves were presented by Roberts & Schwarts (1983) and Bryant (1985) using collocation and Fourier transforms, respectively. Experimental investigations have been presented by, for example, Hammack, Scheffner & Segur (1989), Hammack, Henderson & Segur (2005) and Kimmoun, Ioualalen & Kharif (1999).

The theoretical description of irregular multi-directional waves is much less developed, this is most probably due to the increased complexity. Sharma & Dean

(1981) were the first to derive a second-order solution for bichromatic bi-directional water waves, and this solution is the kernel of second-order irregular wave theory which is obtained by double summation over pairs over interacting bichromatic waves. Inspired by this work, a large number of papers have concentrated on the development of second-order wavemaker theory for unidirectional and multi-directional irregular waves (see e.g. Schäffer, 1996; Schäffer & Steenberg, 2003). However, beyond second-order, theoretical descriptions of irregular waves are rare.

Longuet-Higgins & Phillips (1962) were the first to consider the problem of two deep-water gravity waves travelling at an angle to each other, and they derived a third-order expression for the resulting phase velocity modification due to mutual interaction. A misprint in their general expression was later corrected by Hogan, Gruman & Stiassnie (1988), who generalized their work to bi-directional gravity–capillary waves in deep water. A third-order solution for the sum of two and three collinear deep-water wavetrains was attempted by Pierson (1993), but his dispersion relation was based on intuition rather than on consistent perturbation principles and his results are incorrect. Zhang & Chen (1999) derived a third-order solution for the interaction of three collinear deep-water wave components. This solution forms the kernel of third-order irregular collinear wave theory, which is obtained by triple summation over triplets of interacting waves. Unfortunately, their theory is limited in practice by the assumption that all wave components can be approximated by infinite-depth expressions, which means that not only the primary waves but also their interactions (involving sum and difference frequencies) take place in infinite depth. We shall discuss this limitation in § 4.2.

In the present work, we derive a third-order perturbation solution for bichromatic bi-directional water waves in finite depth. The solution includes explicit expressions for the surface elevation, the amplitude dispersion and the vertical variation of the velocity potential, while the effect of an ambient current is also taken into account, with the option of specifying zero net volume flux. The solution is an extension of Sharma & Dean (1981) from second order to third order, it is an extension of Hsu *et al.* (1979) from monochromatic to bichromatic short-crested waves, and it is an extension of Zhang & Chen (1999) from collinear interactions in deep water to directional interactions in finite depth.

We do acknowledge, that the Zakharov formulation (e.g. as given by Zakharov 1968, 1999; Stiassnie & Shemer 1984; Krasitskii 1994), in principle, allows us to obtain third-order expressions for steady bichromatic bi-directional waves. The direct outcome of such an evaluation is the surface elevation and the velocity potential at the free surface. However, to establish the velocity field, we must invoke successive approximations where the relationship between the potential at the free surface and at the still-water level is inverted. Zhang & Chen (1999) made this evaluation for bichromatic waves in infinite depth (in a single horizontal dimension), but so far, generalized expressions valid in finite depth have not been established.

We also acknowledge that expressions for the nonlinear dispersion relation, involving several interacting waves in finite depth, have previously been given in the framework of the Zakharov kernel function $T(\boldsymbol{k}_1, \boldsymbol{k}_2, \boldsymbol{k}_3, \boldsymbol{k}_4)$, for example, by Stiassnie & Shemer (1984) and Agnon (1993). This kernel function must be evaluated for pair-wise identical wavenumber vectors, i.e. $T_{12} = T(\boldsymbol{k}_1, \boldsymbol{k}_2, \boldsymbol{k}_1 + \boldsymbol{\delta}_1, \boldsymbol{k}_2 + \boldsymbol{\delta}_2)$ and for identical wavenumber vectors $T_{11} = T(\boldsymbol{k}_1 + \boldsymbol{\delta}_1, \boldsymbol{k}_1 + \boldsymbol{\delta}_2, \boldsymbol{k}_1 + \boldsymbol{\delta}_3, \boldsymbol{k}_1 + \boldsymbol{\delta}_4)$, where $\boldsymbol{\delta}_n$ for $n = 1, 2, 3, 4$ denote perturbation vectors approaching zero during the limiting process. In infinite depth, this limiting process is straightforward and explicit expressions can be found (see e.g. Hogan *et al.* 1988 & Zakharov 1999). However, in finite depth,

it turns out that the Zakharov kernel function does not have a unique limit, and that the limit depends on the direction of the perturbation vectors $\boldsymbol{\delta}_n$. So far, only Janssen & Onorato (2005) have addressed this problem, and only for the case of monochromatic unidirectional waves in finite depth. The new theory provided in this paper may serve as a reference for future work on the extension and application of the Zakharov formulations to finite water depth.

The present paper is organized in the following way. First, the governing equations and the perturbation method are defined in § 2. Secondly, the third-order solution for bichromatic bi-directional waves in finite depth is derived in § 3, which also includes a subsection on the identification and removal of singularities and a simple application of the theory. Thirdly, a discussion of the nonlinear dispersion relation is given in § 4, which includes comparisons with the infinite-depth bichromatic solutions by Hogan *et al.* (1988) and Zhang & Chen (1999), the finite-depth bichromatic solution by Agnon (1993), the finite-depth monochromatic short-crested solution by Hsu *et al.* (1979) and the infinite-depth monochromatic short-crested hig-order solution by Roberts (1983). In § 5, we compute third-order resonance curves for unidirectional carrier waves and their three-dimensional perturbation satellites. These curves are compared to the location of the dominant class I and class II wave instabilities determined by the numerical method of McLean (1982). In § 6, we compute the third-order resonance curves for class III Bragg scattering, and the curves are compared to numerical results obtained by Liu & Yue (1998) and Madsen, Fuhrman & Wang (2006). Concluding remarks are given in § 7, with some additional results provided in the Appendix.

## 2. The governing equations and the perturbation method

### 2.1. *Equations for fully nonlinear water waves*

We consider the irrotational flow of an incompressible inviscid fluid with a free surface and a horizontal bottom, and adopt a Cartesian coordinate system with the $x$-axis and the $y$-axis located on the *mean water plane* (MWP) and with the $z$-axis pointing vertically upwards. The fluid domain is bounded by the horizontal sea bed at $z=-h$ and by the free surface $z=\eta(x,y,t)$, and the irrotationality of the flow is expressed through the introduction of the velocity potential $\Phi$ defined by

$$u(x,y,z,t)\equiv\frac{\partial\Phi}{\partial x},\quad v(x,y,z,t)\equiv\frac{\partial\Phi}{\partial y},\quad w(x,y,z,t)\equiv\frac{\partial\Phi}{\partial z},$$

where $u, v$ and $w$ are the components of the particle velocity in the $x, y$ and $z$ directions, respectively. Now, the governing equations for the fully nonlinear wave problem consist of two linear equations (the Laplace equation and the kinematic bottom condition)

$$\frac{\partial^2\Phi}{\partial x^2}+\frac{\partial^2\Phi}{\partial y^2}+\frac{\partial^2\Phi}{\partial z^2}=0\quad\text{for}-h\leqslant z\leqslant\eta(x,y,t),\tag{1}$$

$$\frac{\partial\Phi}{\partial z}=0\quad\text{at}\quad z=-h,\tag{2}$$

and two nonlinear equations (the kinematic and dynamic surface conditions)

$$\frac{\partial\eta}{\partial t}-\frac{\partial\Phi}{\partial z}+\frac{\partial\Phi}{\partial x}\frac{\partial\eta}{\partial x}+\frac{\partial\Phi}{\partial y}\frac{\partial\eta}{\partial y}=0\ \text{at}\ z=\eta(x,y,t),\tag{3}$$

$$\frac{\partial\Phi}{\partial t}+g\eta+\frac{1}{2}\left(\left(\frac{\partial\Phi}{\partial x}\right)^2+\left(\frac{\partial\Phi}{\partial y}\right)^2+\left(\frac{\partial\Phi}{\partial z}\right)^2\right)=0\ \text{at}\ z=\eta(x,y,t).\tag{4}$$

We introduce the following variables defined directly on the free surface:

$$\widetilde{u} \equiv u(x, y, \eta, t) \equiv \left(\frac{\partial \Phi}{\partial x}\right)_{z=\eta}, \quad \widetilde{v} \equiv v(x, y, \eta, t) \equiv \left(\frac{\partial \Phi}{\partial y}\right)_{z=\eta}, \tag{5}$$

$$\widetilde{w} \equiv w(x, y, \eta, t) \equiv \left(\frac{\partial \Phi}{\partial z}\right)_{z=\eta}, \quad \widetilde{\Psi} \equiv \left(\frac{\partial \Phi}{\partial t}\right)_{z=\eta}, \tag{6}$$

by which the nonlinear surface equations (3) and (4) can be reformulated to

$$\frac{\partial \eta}{\partial t} - \widetilde{w} + \widetilde{u}\frac{\partial \eta}{\partial x} + \widetilde{v}\frac{\partial \eta}{\partial y} = 0, \tag{7}$$

$$\widetilde{\Psi} + g\eta + \tfrac{1}{2}(\widetilde{u}^2 + \widetilde{v}^2 + \widetilde{w}^2) = 0. \tag{8}$$

### 2.2. *The perturbation method combined with Taylor series expansions*

In order to derive analytical solutions to the governing equations, we adopt the classical perturbation method, which assumes that some parameter ($\varepsilon$) naturally appearing in the equations, in our case the nonlinearity, is small. Often this analysis is performed in dimensionless variables, in which case $\varepsilon$ represents a given physical quantity such as the wavenumber multiplied by the wave amplitude ($ka$) or the wave amplitude divided by the water depth ($a/h$). We prefer, however, to perform the analysis in dimensional variables, in which case $\varepsilon$ has no physical meaning, but merely appears as a marker convenient for collecting terms of various orders of magnitude. Once the different solutions have been obtained, $\varepsilon$ will be ignored.

An important part of the perturbation method is to express the velocity variables at the free surface in terms of Taylor series expansions from the mean water datum $z = 0$. Including the first three terms in this expansion, we obtain

$$\widetilde{u} \simeq \left(\frac{\partial \Phi}{\partial x} + \eta\frac{\partial^2 \Phi}{\partial x \partial z} + \tfrac{1}{2}\eta^2\frac{\partial^3 \Phi}{\partial x \partial z^2} + \cdots.\right)_{z=0}, \tag{9}$$

$$\widetilde{v} \simeq \left(\frac{\partial \Phi}{\partial y} + \eta\frac{\partial^2 \Phi}{\partial y \partial z} + \tfrac{1}{2}\eta^2\frac{\partial^3 \Phi}{\partial y \partial z^2} + \cdots.\right)_{z=0}, \tag{10}$$

$$\widetilde{w} \simeq \left(\frac{\partial \Phi}{\partial z} + \eta\frac{\partial^2 \Phi}{\partial z^2} + \tfrac{1}{2}\eta^2\frac{\partial^3 \Phi}{\partial z^3} + \cdots.\right)_{z=0}, \tag{11}$$

$$\widetilde{\Psi} \simeq \left(\frac{\partial \Phi}{\partial t} + \eta\frac{\partial^2 \Phi}{\partial t \partial z} + \tfrac{1}{2}\eta^2\frac{\partial^3 \Phi}{\partial t \partial z^2} + \cdots.\right)_{z=0}. \tag{12}$$

## 3. New solution for bichromatic bi-directional waves

### 3.1. *First-order expressions*

As a starting point for the perturbation method, we consider a first-order *bi-directional bichromatic progressive* wave group made up of the two frequencies $\omega_n$ and $\omega_m$. The corresponding wavenumber vectors are defined by $\boldsymbol{k}_n \equiv (k_{nx}, k_{ny})$ and $\boldsymbol{k}_m \equiv (k_{mx}, k_{my})$, and we express the first-order wave solutions by

$$\eta^{(1)} = \varepsilon\,(a_n \cos\theta_n + b_n \sin\theta_n) + \varepsilon(a_m \cos\theta_m + b_m \sin\theta_m), \tag{13}$$

$$\begin{aligned}\Phi^{(1)} = {} & \boldsymbol{U} \cdot \boldsymbol{x} + \varepsilon F_n \cosh\kappa_n(z+h)\,(a_n \sin\theta_n - b_n \cos\theta_n) \\ & + \varepsilon F_m \cosh\kappa_m(z+h)(a_m \sin\theta_m - b_m \cos\theta_m),\end{aligned} \tag{14}$$

where $\boldsymbol{U}$ is an ambient current vector (constant in time and space), $\boldsymbol{x} \equiv (x, y)$ and the phase functions are given by

$$\theta_n \equiv \omega_n t - k_{nx}x - k_{ny}y, \tag{15}$$

$$\theta_m \equiv \omega_m t - k_{mx}x - k_{my}y. \tag{16}$$

For later use we introduce the amplitudes

$$c_n \equiv \sqrt{a_n^2 + b_n^2}, \quad c_m \equiv \sqrt{a_m^2 + b_m^2}. \tag{17}$$

By inserting (14) into the Laplace equation (1), we obtain

$$\kappa_n = |\boldsymbol{k}_n| = \sqrt{k_{nx}^2 + k_{ny}^2}, \quad \kappa_m = |\boldsymbol{k}_m| = \sqrt{k_{mx}^2 + k_{my}^2}, \tag{18}$$

while the kinematic bottom condition (2) is automatically satisfied.

The remaining problem is to consider the nonlinear surface equations (7) and (8). We insert (13) and (14) into (9)–(12), which again are substituted into (7) and (8). Next, we collect terms of order $O(\varepsilon)$ and obtain two independent homogeneous equations. These are satisfied by the linear dispersion relations including a Doppler shift from the ambient current

$$\omega_n = \boldsymbol{k}_n \cdot \boldsymbol{U} + \omega_{1n}, \quad \omega_{1n} \equiv \sqrt{g\kappa_n \tanh h\kappa_n}, \tag{19}$$

$$\omega_m = \boldsymbol{k}_m \cdot \boldsymbol{U} + \omega_{1m}, \quad \omega_{1m} \equiv \sqrt{g\kappa_m \tanh h\kappa_m}, \tag{20}$$

and by

$$F_n = \frac{-\omega_{1n}}{\kappa_n \sinh h\kappa_n}, \quad F_m = \frac{-\omega_{1m}}{\kappa_m \sinh h\kappa_m}. \tag{21}$$

### 3.2. *Second-order solution*

The second-order solution for progressive bi-directional bichromatic waves was first given by Sharma & Dean (1981). Their solution is rederived in this section as an intermediate step towards the new third-order solution given in § 3.3.

In the derivation of the second-order surface elevation and the velocity potential, it turns out to be convenient to start with the following pre-assessment. First, we calculate

$$\begin{aligned}\frac{1}{h}\left(\eta^{(1)}\right)^2 = {} & \varepsilon^2(A_{nm}^- \cos(\theta_n - \theta_m) + B_{nm}^- \sin(\theta_n - \theta_m)) \\ & + \varepsilon^2(A_{nm}^+ \cos(\theta_n + \theta_m) + B_{nm}^+ \sin(\theta_n + \theta_m)) \\ & + \varepsilon^2(A_{2n} \cos 2\theta_n + B_{2n} \sin 2\theta_n + A_{2m} \cos 2\theta_m + B_{2m} \sin 2\theta_m),\end{aligned}$$

where the second-order amplitudes read

$$A_{nm}^{\pm} = \frac{1}{h}(a_n a_m \mp b_n b_m), \quad B_{nm}^{\pm} = \frac{1}{h}(a_m b_n \pm a_n b_m), \tag{22}$$

$$A_{2n} = \frac{1}{2h}\left(a_n^2 - b_n^2\right), \qquad B_{2n} = \frac{1}{h}a_n b_n, \tag{23}$$

with equivalent expressions for $A_{2m}$ and $B_{2m}$. Notice that the contributions from the sum/difference frequencies are found by using the upper/lower signs in (22). This simple calculation is relevant, because the governing equations involve quadratic nonlinearities, and it defines the form (but not the magnitude) of the second-order surface elevation. Now having the form of $\eta^{(2)}$, we can also establish the form (but again not the magnitude) of the second-order velocity potential, simply by using the linear relationship $g\eta \simeq -(\Phi_t)_{(z=0)}$ from (4).

On the basis of this pre-assessment, we now look for second-order bound solutions expressed by

$$\begin{aligned}\eta^{(2)} &= \varepsilon^2 G^-_{nm}(A^-_{nm}\cos(\theta_n-\theta_m)+B^-_{nm}\sin(\theta_n-\theta_m))\\ &+\varepsilon^2 G^+_{nm}(A^+_{nm}\cos(\theta_n+\theta_m)+B^+_{nm}\sin(\theta_n+\theta_m))\\ &+\varepsilon^2 G_{2n}(A_{2n}\cos 2\theta_n+B_{2n}\sin 2\theta_n)+\varepsilon^2 G_{2m}(A_{2m}\cos 2\theta_m+B_{2m}\sin 2\theta_m),\end{aligned} \tag{24}$$

$$\begin{aligned}\Phi^{(2)} &= \varepsilon^2 F^-_{nm}\cosh\kappa^-_{nm}(z+h)(A^-_{nm}\sin(\theta_n-\theta_m)-B^-_{nm}\cos(\theta_n-\theta_m))\\ &+\varepsilon^2 F^+_{nm}\cosh\kappa^+_{nm}(z+h)(A^+_{nm}\sin(\theta_n+\theta_m)-B^+_{nm}\cos(\theta_n+\theta_m))\\ &+\varepsilon^2 F_{2n}\cosh 2\kappa_n(z+h)(A_{2n}\sin 2\theta_n-B_{2n}\cos 2\theta_n)\\ &+\varepsilon^2 F_{2m}\cosh 2\kappa_m(z+h)(A_{2m}\sin 2\theta_m-B_{2m}\cos 2\theta_m),\end{aligned} \tag{25}$$

where $G^-_{nm}$, $G^+_{nm}$, $G_{2n}$, $G_{2m}$, $F^-_{nm}$, $F^+_{nm}$, $F_{2n}$, $F_{2m}$ are unknown transfer functions and $\kappa^-_{nm}$, $\kappa^+_{nm}$ are unknown wavenumbers to be determined.

Inserting (25) into the Laplace equation (1) leads to the determination of the sum (upper signs) and difference (lower signs) wavenumbers

$$\kappa^{\pm}_{nm} = |\boldsymbol{k}_n \pm \boldsymbol{k}_m| = \sqrt{(k_{nx}\pm k_{mx})^2+(k_{ny}\pm k_{my})^2}. \tag{26}$$

Again, the kinematic bottom condition (2) is automatically satisfied. Therefore we concentrate on satisfying the nonlinear surface conditions, i.e. we insert (13)–(14) and (24)–(25) into (9)–(12), which again are substituted into (7) and (8). Terms of order $O(\varepsilon^2)$ are collected and as a result, we obtain algebraic equations for the determination of $G^-_{nm}$, $G^+_{nm}$, $G_{2n}$, $G_{2m}$, $F^-_{nm}$, $F^+_{nm}$, $F_{2n}$ and $F_{2m}$. The self–self interaction solutions read

$$G_{2n} = \tfrac{1}{2}h\kappa_n(2+\cosh 2h\kappa_n)\frac{\coth h\kappa_n}{\sinh^2 h\kappa_n}, \quad F_{2n} = -\frac{3}{4}\frac{h\omega_{1n}}{\sinh^4 h\kappa_n}, \tag{27}$$

with equivalent expressions for $G_{2m}$ and $F_{2m}$. These are the well-known second-order solutions for monochromatic waves. The transfer functions for the sub- and super-harmonic interactions are more involved and can be expressed by

$$G^+_{nm} = \delta_{nm}\Lambda_2(\omega_{1n},\boldsymbol{k}_n,\kappa_n,\omega_{1m},\boldsymbol{k}_m,\kappa_m,\kappa^+_{nm}), \tag{28}$$

$$G^-_{nm} = \Lambda_2(\omega_{1n},\boldsymbol{k}_n,\kappa_n,-\omega_{1m},-\boldsymbol{k}_m,\kappa_m,\kappa^-_{nm}), \tag{29}$$

$$F^+_{nm} = \delta_{nm}\Gamma_2(\omega_{1n},\boldsymbol{k}_n,\kappa_n,\omega_{1m},\boldsymbol{k}_m,\kappa_m,\kappa^+_{nm}), \tag{30}$$

$$F^-_{nm} = \Gamma_2(\omega_{1n},\boldsymbol{k}_n,\kappa_n,-\omega_{1m},-\boldsymbol{k}_m,\kappa_m,\kappa^-_{nm}), \tag{31}$$

where

$$\delta_{nm} = \begin{cases} 1 & \text{for } n\neq m,\\ \frac{1}{2} & \text{for } n=m.\end{cases} \tag{32}$$

The function $\Lambda_2$ used for the determination of $G^+_{nm}$ and $G^-_{nm}$ is defined by

$$\begin{aligned}&\Lambda_2(\omega_{1n},\boldsymbol{k}_n,\kappa_n,\omega_{1m},\boldsymbol{k}_m,\kappa_m,\kappa^+_{nm})\\ &\equiv \frac{gh}{\beta_{nm}}(\omega_{1n}+\omega_{1m})\cosh h\kappa^+_{nm}\left(\omega_{1n}\left(\kappa_m^2+\boldsymbol{k}_n\cdot\boldsymbol{k}_m\right)+\omega_{1m}\left(\kappa_n^2+\boldsymbol{k}_n\cdot\boldsymbol{k}_m\right)\right)\\ &+\frac{h\kappa^+_{nm}}{\beta_{nm}}\sinh h\kappa^+_{nm}\left(g^2\boldsymbol{k}_n\cdot\boldsymbol{k}_m+\omega_{1n}^2\omega_{1m}^2-\omega_{1n}\omega_{1m}(\omega_{1n}+\omega_{1m})^2\right),\end{aligned} \tag{33}$$

where

$$\beta_{nm} \equiv 2\omega_{1n}\omega_{1m}((\omega_{1n}+\omega_{1m})^2 \cosh h\kappa_{nm}^{+} - g\kappa_{nm}^{+} \sinh h\kappa_{nm}^{+}), \tag{34}$$

which is to be considered as a local variable. Similarly, the function $\Gamma_2$ used for the determination of $F_{nm}^{+}$ and $F_{nm}^{-}$ is defined by

$$\begin{aligned}\Gamma_2\,&(\omega_{1n}, \boldsymbol{k}_n, \kappa_n, \omega_{1m}, \boldsymbol{k}_m, \kappa_m, \kappa_{nm}^{+})\\ &\equiv \frac{h}{\beta_{nm}}(\omega_{1n}\omega_{1m}(\omega_{1n}+\omega_{1m})((\omega_{1n}+\omega_{1m})^2 - \omega_{1n}\omega_{1m}))\\ &\quad - \frac{hg^2}{\beta_{nm}}\left(\omega_{1n}\left(\kappa_m^2 + 2\boldsymbol{k}_n\cdot\boldsymbol{k}_m\right) + \omega_{1m}\left(\kappa_n^2 + 2\boldsymbol{k}_n\cdot\boldsymbol{k}_m\right)\right).\end{aligned} \tag{35}$$

For later use, we emphasize that according to (26), and (28)–(31) we have the following second-order relations

$$\kappa_{mn}^{\pm} = \kappa_{nm}^{\pm}, \quad G_{mn}^{\pm} = G_{nm}^{\pm}, \quad F_{mn}^{\pm} = \pm F_{nm}^{\pm}. \tag{36}$$

Note that the second-order transfer functions for bichromatic bi-directional waves defined by (28)–(31) with (33) and (35) are identical to the solution given by Sharma & Dean (1981). Schäffer & Steenberg (2003) also gave this solution in connection with the development of a second-order wavemaker theory for multi-directional waves. Unfortunately, a typographical error appears in their formulation; the last term in their equation (65) should be $\omega_n^2 + \omega_m^2$ rather than $\omega_n^2 \pm \omega_m^2$.

### 3.3. *Third-order solution*

In this section, we derive the new third-order solution for bi-directional bichromatic waves. In this process, it is again convenient to start with a pre-assessment of the third-order expressions by calculating $(1/h)(\eta^{(1)}+\eta^{(2)})^2$ while collecting terms of order $\varepsilon^3$. This yields

$$\begin{aligned}&\varepsilon^3\,(G_{2m} + 2G_{nm}^{+})(A_{n2m}^{+}\cos(\theta_n + 2\theta_m) + B_{n2m}^{+}\sin(\theta_n + 2\theta_m))\\ &\quad + \varepsilon^3(G_{2m} + 2G_{nm}^{-})(A_{n2m}^{-}\cos(\theta_n - 2\theta_m) + B_{n2m}^{-}\sin(\theta_n - 2\theta_m))\\ &\quad + \varepsilon^3(G_{2n} + 2G_{nm}^{+})(A_{m2n}^{+}\cos(\theta_m + 2\theta_n) + B_{m2n}^{+}\sin(\theta_m + 2\theta_n))\\ &\quad + \varepsilon^3(G_{2n} + 2G_{nm}^{-})(A_{m2n}^{-}\cos(\theta_m - 2\theta_n) + B_{m2n}^{-}\sin(\theta_m - 2\theta_n))\\ &\quad + \varepsilon^3 G_{2n}(A_{3n}\cos 3\theta_n + B_{3n}\sin 3\theta_n)\\ &\quad + \varepsilon^3 G_{2m}(A_{3m}\cos 3\theta_m + B_{3m}\sin 3\theta_m)\\ &\quad + \varepsilon^3(A_n\cos\theta_n + B_n\sin\theta_n + A_m\cos\theta_m + B_m\sin\theta_m),\end{aligned}$$

where the third-order amplitudes read

$$A_{n2m}^{\pm} = \frac{a_n\left(a_m^2 - b_m^2\right) \mp 2b_n a_m b_m}{2h^2}, \quad B_{n2m}^{\pm} = \frac{b_n\left(a_m^2 - b_m^2\right) \pm 2a_n a_m b_m}{2h^2}, \tag{37}$$

$$A_{m2n}^{\pm} = \frac{a_m\left(a_n^2 - b_n^2\right) \mp 2b_m a_n b_n}{2h^2}, \quad B_{m2n}^{\pm} = \frac{b_m\left(a_n^2 - b_n^2\right) \pm 2a_m a_n b_n}{2h^2}, \tag{38}$$

$$A_{3n} = \frac{a_n\left(a_n^2 - 3b_n^2\right)}{2h^2}, \qquad B_{3n} = \frac{b_n\left(3a_n^2 - b_n^2\right)}{2h^2}. \tag{39}$$

The expressions for $A_{3m}$ and $B_{3m}$ are analogous to the expressions for $A_{3n}$ and $B_{3n}$, while the expressions for $A_n$, $B_n$, $A_m$ and $B_m$ are omitted because they will not appear in the bound third-order solution. Again this calculation defines the form (but not the magnitude) of the third-order surface elevation. Having the form of $\eta^{(3)}$, we establish

the form (but not the magnitude) of the third-order velocity potential using the linear relationship $g\eta \simeq -(\Phi_t)_{(z=0)}$ from (4).

On the basis of this pre-assessment, we now look for third-order bound solutions expressed by

$$\begin{aligned}\eta^{(3)} = {} & \varepsilon^3 G^+_{n2m}(A^+_{n2m}\cos(\theta_n + 2\theta_m) + B^+_{n2m}\sin(\theta_n + 2\theta_m)) \\ & + \varepsilon^3 G^-_{n2m}(A^-_{n2m}\cos(\theta_n - 2\theta_m) + B^-_{n2m}\sin(\theta_n - 2\theta_m)) \\ & + \varepsilon^3 G^+_{m2n}(A^+_{m2n}\cos(\theta_m + 2\theta_n) + B^+_{m2n}\sin(\theta_m + 2\theta_n)) \\ & + \varepsilon^3 G^-_{m2n}(A^-_{m2n}\cos(\theta_m - 2\theta_n) + B^-_{m2n}\sin(\theta_m - 2\theta_n)) \\ & + \varepsilon^3 G_{3n}(A_{3n}\cos 3\theta_n + B_{3n}\sin 3\theta_n) \\ & + \varepsilon^3 G_{3m}(A_{3m}\cos 3\theta_m + B_{3m}\sin 3\theta_m),\end{aligned} \tag{40}$$

and

$$\begin{aligned}\Phi^{(3)} = {} & \varepsilon^3 F^+_{n2m}\cosh\kappa^+_{n2m}(z+h)(A^+_{n2m}\sin(\theta_n + 2\theta_m) - B^+_{n2m}\cos(\theta_n + 2\theta_m)) \\ & + \varepsilon^3 F^-_{n2m}\cosh\kappa^-_{n2m}(z+h)(A^-_{n2m}\sin(\theta_n - 2\theta_m) - B^-_{n2m}\cos(\theta_n - 2\theta_m)) \\ & + \varepsilon^3 F^+_{m2n}\cosh\kappa^+_{m2n}(z+h)(A^+_{m2n}\sin(\theta_m + 2\theta_n) - B^+_{m2n}\cos(\theta_m + 2\theta_n)) \\ & + \varepsilon^3 F^-_{m2n}\cosh\kappa^-_{m2n}(z+h)(A^-_{m2n}\sin(\theta_m - 2\theta_n) - B^-_{m2n}\cos(\theta_m - 2\theta_n)) \\ & + \varepsilon^3 F_{3n}\cosh 3\kappa_n(z+h)(A_{3n}\sin 3\theta_n - B_{3n}\cos 3\theta_n) \\ & + \varepsilon^3 F_{3m}\cosh 3\kappa_m(z+h)(A_{3m}\sin 3\theta_m - B_{3m}\cos 3\theta_m) \\ & + \varepsilon^3 F_{13n}\cosh\kappa_n(z+h)(a_n\sin\theta_n - b_n\cos\theta_n) \\ & + \varepsilon^3 F_{13m}\cosh\kappa_m(z+h)(a_m\sin\theta_m - b_m\cos\theta_m),\end{aligned} \tag{41}$$

where $G^{\pm}_{n2m}$, $G^{\pm}_{m2n}$, $G_{3n}$, $G_{3m}$, $F^{\pm}_{n2m}$, $F^{\pm}_{m2n}$, $F_{3n}$, $F_{3m}$, $F_{13n}$, $F_{13m}$ are unknown transfer functions and $\kappa^{\pm}_{n2m}$, $\kappa^{\pm}_{m2n}$ are unknown wavenumbers to be determined.

At third order, the phase functions (15) and (16) now incorporate the frequencies

$$\omega_n = \boldsymbol{k}_n \cdot \boldsymbol{U} + \omega_{1n}(1 + \varepsilon^2\omega_{3n}), \tag{42}$$

$$\omega_m = \boldsymbol{k}_m \cdot \boldsymbol{U} + \omega_{1m}(1 + \varepsilon^2\omega_{3m}), \tag{43}$$

where $\omega_{3n}$ and $\omega_{3m}$ define the third-order amplitude dispersion, which is necessary in order to remove secular terms from the expansion. In order to determine the wavenumbers, we insert (41) into the Laplace equation (1) and obtain

$$\kappa^{\pm}_{n2m} = |\boldsymbol{k}_n \pm 2\boldsymbol{k}_m| = \sqrt{(k_{nx} \pm 2k_{mx})^2 + (k_{ny} \pm 2k_{my})^2}, \tag{44}$$

$$\kappa^{\pm}_{m2n} = |\boldsymbol{k}_m \pm 2\boldsymbol{k}_n| = \sqrt{(k_{mx} \pm 2k_{nx})^2 + (k_{my} \pm 2k_{ny})^2}. \tag{45}$$

Again, the kinematic bottom condition (2) is automatically satisfied by (41). Therefore we concentrate on satisfying the nonlinear surface conditions, i.e. we insert (13)–(14), (24)–(25) and (40)–(41) into (9)–(12), which again are substituted into (7) and (8). Terms of $O(\varepsilon^3)$ are collected and as a result, we obtain algebraic equations for the determination of $G^{\pm}_{n2m}$, $G^{\pm}_{m2n}$, $G_{3n}$, $G_{3m}$, $F^{\pm}_{n2m}$, $F^{\pm}_{m2n}$, $F_{3n}$ and $F_{3m}$. The self–self–self interaction solutions read

$$G_{3n} = \frac{3}{128}\frac{h^2\kappa_n^2}{\sinh^6 h\kappa_n}(14 + 15\cosh 2h\kappa_n + 6\cosh 4h\kappa_n + \cosh 6h\kappa_n), \tag{46}$$

$$F_{3n} = \frac{1}{32}\frac{h^2\kappa_n\omega_{1n}}{\sinh^7 h\kappa_n}(-11 + 2\cosh 2h\kappa_n), \tag{47}$$

with equivalent expressions for $G_{3m}$ and $F_{3m}$. These are the well-known Stokes solutions for monochromatic waves. The transfer functions for the third-order sum- and difference-interactions are more involved and can be expressed by the functions

$$G^+_{n2m} = \delta_{n2m}\Lambda_3(\omega_{1n}, \boldsymbol{k}_n, \kappa_n, \omega_{1m}, \boldsymbol{k}_m, \kappa_m, \kappa^+_{nm}, \kappa^+_{n2m}, G^+_{nm}, F^+_{nm}), \tag{48}$$

$$G^+_{m2n} = \delta_{m2n}\Lambda_3(\omega_{1m}, \boldsymbol{k}_m, \kappa_m, \omega_{1n}, \boldsymbol{k}_n, \kappa_n, \kappa^+_{mn}, \kappa^+_{m2n}, G^+_{mn}, F^+_{mn}), \tag{49}$$

$$G^-_{n2m} = \Lambda_3(\omega_{1n}, \boldsymbol{k}_n, \kappa_n, -\omega_{1m}, -\boldsymbol{k}_m, \kappa_m, \kappa^-_{nm}, \kappa^-_{n2m}, G^-_{nm}, F^-_{nm}), \tag{50}$$

$$G^-_{m2n} = \Lambda_3(\omega_{1m}, \boldsymbol{k}_m, \kappa_m, -\omega_{1n}, -\boldsymbol{k}_n, \kappa_n, \kappa^-_{mn}, \kappa^-_{m2n}, G^-_{mn}, F^-_{mn}), \tag{51}$$

$$F^+_{n2m} = \delta_{n2m}\Gamma_3(\omega_{1n}, \boldsymbol{k}_n, \kappa_n, \omega_{1m}, \boldsymbol{k}_m, \kappa_m, \kappa^+_{nm}, \kappa^+_{n2m}, G^+_{nm}, F^+_{nm}), \tag{52}$$

$$F^+_{m2n} = \delta_{m2n}\Gamma_3(\omega_{1m}, \boldsymbol{k}_m, \kappa_m, \omega_{1n}, \boldsymbol{k}_n, \kappa_n, \kappa^+_{mn}, \kappa^+_{m2n}, G^+_{mn}, F^+_{mn}), \tag{53}$$

$$F^-_{n2m} = \Gamma_3(\omega_{1n}, \boldsymbol{k}_n, \kappa_n, -\omega_{1m}, -\boldsymbol{k}_m, \kappa_m, \kappa^-_{nm}, \kappa^-_{n2m}, G^-_{nm}, F^-_{nm}), \tag{54}$$

$$F^-_{m2n} = \Gamma_3(\omega_{1m}, \boldsymbol{k}_m, \kappa_m, -\omega_{1n}, -\boldsymbol{k}_n, \kappa_n, \kappa^-_{mn}, \kappa^-_{m2n}, G^-_{mn}, F^-_{mn}), \tag{55}$$

where

$$\delta_{n2m} = \delta_{m2n} = \begin{cases} 1 & \text{for } n \neq m, \\ \frac{1}{3} & \text{for } n = m. \end{cases} \tag{56}$$

The function $\Lambda_3$ used for the determination of $G^{\pm}_{n2m}$ and $G^{\pm}_{m2n}$ is defined by

$$\begin{aligned}
&\Lambda_3(\omega_{1n}, \boldsymbol{k}_n, \kappa_n, \omega_{1m}, \boldsymbol{k}_m, \kappa_m, \kappa^+_{nm}, \kappa^+_{n2m}, G^+_{nm}, F^+_{nm}) \\
&\quad\equiv \frac{G^+_{nm}}{\beta_{n2m}}\left(gh\left(2\kappa_m^2 + \boldsymbol{k}_n\cdot\boldsymbol{k}_m\right)\alpha_{n2m} - h\omega_{1m}^3\gamma_{n2m}\right) \\
&\quad- \frac{F^+_{nm}}{\beta_{n2m}}(\cosh h\kappa^+_{nm}\left(h\omega_{1m}\alpha_{n2m}\left(2\kappa_m^2 + \kappa_n^2 + 3\boldsymbol{k}_n\cdot\boldsymbol{k}_m\right) + gh\gamma_{n2m}\left(\kappa_m^2 + \boldsymbol{k}_n\cdot\boldsymbol{k}_m\right)\right) \\
&\quad- h\omega_{1m}\left(2\omega_{1m} + \omega_{1n}\right)\gamma_{n2m}\kappa^+_{nm}\sinh h\kappa^+_{nm}) \\
&\quad+ \frac{h^2\alpha_{n2m}}{4\beta_{n2m}}\left(\omega_{1m}^2\left(4\kappa_m^2 + 2\boldsymbol{k}_n\cdot\boldsymbol{k}_m\right) + \omega_{1n}\omega_{1m}\left(\kappa_n^2 + 2\boldsymbol{k}_n\cdot\boldsymbol{k}_m\right)\right) \\
&\quad+ \frac{h^2\alpha_{n2m}}{4\omega_{1m}\omega_{1n}\beta_{n2m}}\frac{(2+\cosh 2h\kappa_m)}{\sinh^2 h\kappa_m}g^2\kappa_m^2\left(\kappa_n^2 + 2\boldsymbol{k}_n\cdot\boldsymbol{k}_m\right) \\
&\quad+ \frac{h^2\alpha_{n2m}}{4\beta_{n2m}}\frac{\cosh 2h\kappa_m}{\sinh^4 h\kappa_m}\left(6\kappa_m^2 + 3\boldsymbol{k}_n\cdot\boldsymbol{k}_m\right)\omega_{1m}^2 + \frac{3gh^2\gamma_{n2m}}{4\omega_{1n}\beta_{n2m}}\frac{\cosh 2h\kappa_m}{\sinh^4 h\kappa_m}\omega_{1m}^2\boldsymbol{k}_n\cdot\boldsymbol{k}_m \\
&\quad- \frac{gh^2\gamma_{n2m}}{4\omega_{1n}\beta_{n2m}}\left(\left(2\kappa_n^2 - 2\boldsymbol{k}_n\cdot\boldsymbol{k}_m\right)\omega_{1m}^2 + \left(2\kappa_m^2 + \kappa_n^2\right)\omega_{1m}\omega_{1n} + \left(2\kappa_m^2 - 2\boldsymbol{k}_n\cdot\boldsymbol{k}_m\right)\omega_{1n}^2\right) \\
&\quad- \frac{gh^2\gamma_{n2m}\kappa_m^2}{4\omega_{1m}\beta_{n2m}\sinh^2 h\kappa_m}\left(\omega_{1n}^2\left(2+\cosh 2h\kappa_m\right) + 6\omega_{1m}\left(2\omega_{1m} + \omega_{1n}\right)\right),
\end{aligned} \tag{57}$$

which incorporates the local variables

$$\beta_{n2m} \equiv \omega_{1m}((2\omega_{1m} + \omega_{1n})^2\cosh h\kappa^+_{n2m} - g\kappa^+_{n2m}\sinh h\kappa^+_{n2m}), \tag{58}$$

$$\alpha_{n2m} \equiv (2\omega_{1m} + \omega_{1n})\cosh h\kappa^+_{n2m}, \quad \gamma_{n2m} \equiv \kappa^+_{n2m}\sinh h\kappa^+_{n2m}. \tag{59}$$

Similarly, the function $\Gamma_3$, used for the determination of $F^{\pm}_{n2m}$ and $F^{\pm}_{m2n}$, is defined by

$$\begin{aligned}
&\Gamma_3(\omega_{1n}, \boldsymbol{k}_n, \kappa_n, \omega_{1m}, \boldsymbol{k}_m, \kappa_m, \kappa^+_{nm}, \kappa^+_{n2m}, G^+_{nm}, F^+_{nm}) \\
&\quad\equiv -\frac{G^+_{nm}}{\beta_{n2m}}\left(hg^2\left(2\kappa_m^2 + \boldsymbol{k}_n\cdot\boldsymbol{k}_m\right) - h\omega_{1m}^3\left(2\omega_{1m} + \omega_{1n}\right)\right) \\
&\quad+ \frac{F^+_{nm}}{\beta_{n2m}}gh\cosh h\kappa^+_{nm}\left(\omega_{1m}(\kappa^+_{nm})^2 + \left(3\omega_{1m} + \omega_{1n}\right)\left(\kappa_m^2 + \boldsymbol{k}_n\cdot\boldsymbol{k}_m\right)\right)
\end{aligned}$$

$$
\begin{aligned}
&- \frac{F_{nm}^{+}}{\beta_{n2m}} h\kappa_{nm}^{+}\omega_{1m}\left(2\omega_{1m}+\omega_{1n}\right)^2 \sinh h\kappa_{nm}^{+} + \frac{3gh^2\kappa_m^2\left(2\omega_{1m}+\omega_{1n}\right)^2}{2\beta_{n2m}\sinh^2 h\kappa_m} \\
&- \frac{gh^2}{2\omega_{1n}\beta_{n2m}}\left(\omega_{1n}^2\left(3\omega_{1m}+\omega_{1n}\right)\left(\boldsymbol{k}_n\cdot\boldsymbol{k}_m-\kappa_m^2\right)+2\omega_{1m}^2\left(\omega_{1n}+\omega_{1m}\right)\left(\boldsymbol{k}_n\cdot\boldsymbol{k}_m-\kappa_n^2\right)\right) \\
&- \frac{gh^2\kappa_m^2\left(2+\cosh 2h\kappa_m\right)}{4\omega_{1m}\omega_{1n}\beta_{n2m}\sinh^2 h\kappa_m}\left(g^2\left(2\boldsymbol{k}_n\cdot\boldsymbol{k}_m+\kappa_n^2\right)-\omega_{1n}^3\left(2\omega_{1m}+\omega_{1n}\right)\right) \\
&- \frac{3gh^2\omega_{1m}^2\cosh 2h\kappa_m}{2\omega_{1n}\beta_{n2m}\sinh^4 h\kappa_m}\left(\left(\omega_{1n}+\omega_{1m}\right)\boldsymbol{k}_n\cdot\boldsymbol{k}_m+\omega_{1n}\kappa_m^2\right). \qquad (60)
\end{aligned}
$$

The third-order correction to the first-order potential (necessary to remove secular terms) is determined by

$$F_{13n} = c_n^2\omega_{1n}\kappa_n\left(\frac{-13+24\cosh 2h\kappa_n+\cosh 4h\kappa_n}{64\sinh^5 h\kappa_n}\right)+c_m^2\Upsilon_{13n}, \qquad (61)$$

$$F_{13m} = c_m^2\omega_{1m}\kappa_m\left(\frac{-13+24\cosh 2h\kappa_m+\cosh 4h\kappa_m}{64\sinh^5 h\kappa_m}\right)+c_n^2\Upsilon_{13m}, \qquad (62)$$

where

$$\Upsilon_{13n} = \Upsilon(\omega_{1n}, \boldsymbol{k}_n, \kappa_n, \omega_{1m}, \boldsymbol{k}_m, \kappa_m, \kappa_{nm}^{\pm}, G_{nm}^{\pm}, F_{nm}^{\pm}), \qquad (63)$$

$$\Upsilon_{13m} = \Upsilon(\omega_{1m}, \boldsymbol{k}_m, \kappa_m, \omega_{1n}, \boldsymbol{k}_n, \kappa_n, \kappa_{mn}^{\pm}, G_{mn}^{\pm}, F_{mn}^{\pm}), \qquad (64)$$

and where

$$
\begin{aligned}
&\Upsilon(\omega_{1n}, \boldsymbol{k}_n, \kappa_n, \omega_{1m}, \boldsymbol{k}_m, \kappa_m, \kappa_{nm}^{\pm}, G_{nm}^{\pm}, F_{nm}^{\pm}) \\
&\equiv \frac{g}{4\omega_{1n}\omega_{1m}\cosh h\kappa_n}\left(\omega_{1m}\left(\kappa_n^2-\kappa_m^2\right)-\omega_{1n}\boldsymbol{k}_n\cdot\boldsymbol{k}_m\right) \\
&+ \frac{\left(G_{nm}^{+}+G_{nm}^{-}\right)}{4h\omega_{1n}^2\omega_{1m}\cosh h\kappa_n}\left(g^2\boldsymbol{k}_n\cdot\boldsymbol{k}_m+\omega_{1m}^3\omega_{1n}\right) \\
&- \frac{1}{4h\cosh h\kappa_n}\left(F_{nm}^{+}\kappa_{nm}^{+}\sinh h\kappa_{nm}^{+}+F_{nm}^{-}\kappa_{nm}^{-}\sinh h\kappa_{nm}^{-}\right) \\
&+ \frac{F_{nm}^{+}g\cosh h\kappa_{nm}^{+}}{4h\omega_{1n}^2\omega_{1m}\cosh h\kappa_n}\left(\left(\omega_{1n}+\omega_{1m}\right)\left(\boldsymbol{k}_n\cdot\boldsymbol{k}_m+\kappa_m^2\right)-\omega_{1m}(\kappa_{nm}^{+})^2\right) \\
&+ \frac{F_{nm}^{-}g\cosh h\kappa_{nm}^{-}}{4h\omega_{1n}^2\omega_{1m}\cosh h\kappa_n}\left(\left(\omega_{1n}-\omega_{1m}\right)\left(\boldsymbol{k}_n\cdot\boldsymbol{k}_m-\kappa_m^2\right)-\omega_{1m}(\kappa_{nm}^{-})^2\right). \qquad (65)
\end{aligned}
$$

Finally, the third-order correction to the frequency (necessary to remove secular terms) reads

$$\omega_{3n} = c_n^2\kappa_n^2\left(\frac{8+\cosh 4h\kappa_n}{16\sinh^4 h\kappa_n}\right)+c_m^2\kappa_m^2\Omega_{nm}, \qquad (66)$$

$$\omega_{3m} = c_m^2\kappa_m^2\left(\frac{8+\cosh 4h\kappa_m}{16\sinh^4 h\kappa_m}\right)+c_n^2\kappa_n^2\Omega_{mn}, \qquad (67)$$

where

$$\kappa_m^2\Omega_{nm} = \Omega(\omega_{1n}, \boldsymbol{k}_n, \kappa_n, \omega_{1m}, \boldsymbol{k}_m, \kappa_m, \kappa_{nm}^{\pm}, G_{nm}^{\pm}, F_{nm}^{\pm}), \qquad (68)$$

$$\kappa_n^2\Omega_{mn} = \Omega(\omega_{1m}, \boldsymbol{k}_m, \kappa_m, \omega_{1n}, \boldsymbol{k}_n, \kappa_n, \kappa_{mn}^{\pm}, G_{mn}^{\pm}, F_{mn}^{\pm}), \qquad (69)$$

and

$$\begin{aligned}
&\Omega(\omega_{1n}, \boldsymbol{k}_n, \kappa_n, \omega_{1m}, \boldsymbol{k}_m, \kappa_m, \kappa^{\pm}_{nm}, G^{\pm}_{nm}, F^{\pm}_{nm}) \\
&\quad \equiv \left( \frac{(2\omega_{1m}^2 + \omega_{1n}^2)}{4\omega_{1n}\omega_{1m}} \boldsymbol{k}_n \cdot \boldsymbol{k}_m + \tfrac{1}{4}\kappa_m^2 \right) + (G^{+}_{nm} + G^{-}_{nm}) \left( \frac{g\boldsymbol{k}_n \cdot \boldsymbol{k}_m}{4h\omega_{1n}\omega_{1m}} - \frac{\omega_{1m}^2}{4gh} \right) \\
&\quad + \frac{\omega_{1n}}{4gh} (F^{+}_{nm}\kappa^{+}_{nm} \sinh h\kappa^{+}_{nm} + F^{-}_{nm}\kappa^{-}_{nm} \sinh h\kappa^{-}_{nm}) \\
&\quad - \frac{F^{+}_{nm} \cosh h\kappa^{+}_{nm}}{4h\omega_{1n}\omega_{1m}} \left( (\omega_{1n} - \omega_{1m}) \left( \kappa_m^2 + \boldsymbol{k}_n \cdot \boldsymbol{k}_m \right) + \omega_{1m} (\kappa^{+}_{nm})^2 \right) \\
&\quad + \frac{F^{-}_{nm} \cosh h\kappa^{-}_{nm}}{4h\omega_{1n}\omega_{1m}} \left( (\omega_{1n} + \omega_{1m}) \left( \kappa_m^2 - \boldsymbol{k}_n \cdot \boldsymbol{k}_m \right) - \omega_{1m} (\kappa^{-}_{nm})^2 \right). \qquad (70)
\end{aligned}$$

This completes the third-order theory, which provides explicit expressions for the surface elevation, the amplitude dispersion and the vertical variation of the velocity potential for bichromatic bi-directional water waves in finite depth (expressed in terms of the mean water depth $h$). Note, that in order to use the theory for wave generation in various numerical models, additional expressions for the velocity potential at the free surface are required (see Appendix).

### 3.4. *The time-averaged volume flux*

The time-averaged volume flux vector is defined by

$$\boldsymbol{M} \equiv \overline{\int_{-h}^{0} \nabla \Phi \, \mathrm{d}z} + \overline{\int_{0}^{\eta} \nabla \Phi \, \mathrm{d}z}, \qquad (71)$$

where $\nabla$ is the horizontal gradient operator, while the overbar represents the time-averaging process. Consistent with (9)–(12), we evaluate the second integral in (71) by using Taylor series expansions from $z = 0$, i.e.

$$\overline{\int_{0}^{\eta} \nabla \Phi \, \mathrm{d}z} \simeq \overline{\int_{0}^{\eta} \nabla \left( \Phi + \zeta \frac{\partial \Phi}{\partial z} + \tfrac{1}{2}\zeta^2 \frac{\partial^2 \Phi}{\partial z^2} + \cdots \right)_{z=0} \mathrm{d}\zeta}. \qquad (72)$$

By substituting the expressions for $\Phi^{(1)}$, $\Phi^{(2)}$, $\Phi^{(3)}$ and $\eta^{(1)}$, $\eta^{(2)}$, $\eta^{(3)}$ into (72) and (71), we obtain the result

$$\boldsymbol{M} = h\boldsymbol{U} + \varepsilon^2 \left( \frac{c_n^2 \omega_{1n}}{2\kappa_n} \coth h\kappa_n \right) \boldsymbol{k}_n + \varepsilon^2 \left( \frac{c_m^2 \omega_{1m}}{2\kappa_m} \coth h\kappa_m \right) \boldsymbol{k}_m + O(\varepsilon^4). \qquad (73)$$

Under certain conditions, e.g. in closed wave tanks, $\boldsymbol{M}$ will be zero, and in this case (73) can be used to determine the resulting return current, which becomes

$$\boldsymbol{U} = -\varepsilon^2 \left( \frac{c_n^2 \omega_{1n}}{2h\kappa_n} \coth h\kappa_n \right) \boldsymbol{k}_n - \varepsilon^2 \left( \frac{c_m^2 \omega_{1m}}{2h\kappa_m} \coth h\kappa_m \right) \boldsymbol{k}_m. \qquad (74)$$

### 3.5. *Identification and removal of singularities*

For certain combinations of wavenumbers and wave angles, singularities appear in the transfer functions $G^{-}_{n2m}$, $F^{-}_{n2m}$ and $G^{-}_{m2n}$, $F^{-}_{m2n}$. Similar problems were discussed by Roberts (1983) in connection with monochromatic short-crested waves in infinite depth. The singularities originate from the division by $\beta_{n2m}$ defined in (58) and can be traced to roots in the functions

$$(G^-_{n2m}, F^-_{n2m}): \qquad g\kappa^-_{n2m}\tanh h\kappa^-_{n2m} - (\omega_{1n} - 2\omega_{1m})^2 = 0, \tag{75}$$

$$(G^-_{m2n}, F^-_{m2n}): \qquad g\kappa^-_{m2n}\tanh h\kappa^-_{m2n} - (\omega_{1m} - 2\omega_{1n})^2 = 0, \tag{76}$$

where $\kappa^-_{n2m}$ and $\kappa^-_{m2n}$ are defined in (44) and (45). We note that $\omega_{1n} - 2\omega_{1m}$ and $\omega_{1m} - 2\omega_{1n}$ represent the frequencies of the bound waves with wavenumbers $\kappa^-_{n2m}$ and $\kappa^-_{m2n}$, and that (75) and (76) actually express the mismatches between bound and free wavenumbers in a quartet interaction. Owing to harmonic resonance, these mismatches may go to zero for certain combinations of wavenumbers and wave angles.

In order to analyse (75) and (76), we define the interacting wavenumber vector components by

$$k_{nx} = \kappa(1+\rho)\sin\varphi, \quad k_{ny} = \kappa(1+\rho)\cos\varphi,$$
$$k_{mx} = \kappa(1-\rho)\sin\varphi, \quad k_{my} = -\kappa(1-\rho)\cos\varphi,$$

i.e. $\varphi \to 90^\circ$ corresponds to the collinear limit, while $\varphi \to 0^\circ$ corresponds to the colliding limit. The roots $\varphi_r$ of (75) and (76) are, respectively, shown in figures 1(*a*) and 1(*b*) as functions of $\rho$ for discrete values of $h\kappa$. In general, we notice that $\varphi_r \to 90^\circ$ as $\rho \to 0$, in agreement with the monochromatic case considered by Roberts (1983). The roots of (75) occur for $\rho < 0.4$ and are confined to a narrow region $84^\circ < \varphi_r \leqslant 90^\circ$, which shrinks for decreasing values of $h\kappa$. In contrast, the roots of (76) cover the complete interval $0^\circ \leqslant \varphi_r \leqslant 90^\circ$. In deep water, they occur only for $\rho < 0.6$. As the depth is decreased, this gradually reduces to $\rho < 0.5$ (with $h\kappa = 1.2$), before ultimately growing to encompass the full range of $\rho$ in shallow water.

Alternatively, we may determine the roots $\rho_r$ of (75) and (76) for given wave angles $\varphi$. Based on figures 1(*a*, *b*) we can conclude that (76) will always have one root $\rho_{r,1}$, while (75) will have either two roots $\rho_{r,1}$ and $\rho_{r,2}$ (for $84^\circ < \varphi \leqslant 90^\circ$) or zero roots. It turns out that the singularities are simple poles, and we can generally remove these poles from a function $G$ by using

$$\widetilde{G} = G - \sum_j \frac{b_j}{(\rho - \rho_{r,j})}, \quad b_j = \lim_{\rho\to\rho_{r,j}}\{(\rho - \rho_{r,j})G\}, \tag{77}$$

where the tilde indicates the function after removal of the singularity. By the use of (77) it is straightforward to obtain reliable results for the transfer functions $G^-_{n2m}$, $F^-_{n2m}$ and $G^-_{m2n}$, $F^-_{m2n}$. As an example, Figure 1(*c*) shows the variation of $G^-_{m2n}$ and $\widetilde{G}^-_{m2n}$ as a function of $\rho$ for the case of $\varphi = 40^\circ$ and $\kappa h = 1.2$. We notice that the function $\widetilde{G}^-_{m2n}$ has a smooth behaviour near the original singularity and that it resembles the variation of $G^+_{m2n}$.

### 3.6. *Bichromatic short-crested wave example*

We illustrate the third-order solution by considering the following case of bichromatic short-crested waves in a depth $h = 10\,\mathrm{m}$: $\omega_n = 2\pi \times 0.15\,\mathrm{s}^{-1}$, $a_n = 1.3\,\mathrm{m}$, $\varphi_n = 10^\circ$, $\omega_m = 2\pi \times 0.10\,\mathrm{s}^{-1}$, $a_m = 1.0\,\mathrm{m}$, $\varphi_m = -10^\circ$ where $\boldsymbol{k}_n = \kappa_n(\cos\varphi_n, \sin\varphi_n)$ and $\boldsymbol{k}_m = \kappa_m(\cos\varphi_m, \sin\varphi_m)$. Figure 2(*a*) shows a perspective view of the third-order surface elevation. With angles so close to the collinear limit, the wave pattern actually becomes rather long crested, but nevertheless the surface shape is much more rounded than the equivalent monochromatic long-crested case. Figure 2(*b*) shows the first- and third-order surface elevations along the centreline (i.e. $y = 0$), while figure 2(*c*) shows the first- and third-order velocity profiles at the centrepoint $(x, y) = (0, 0)$. The relevant coefficients corresponding to figures 2(*a*)(*c*) are given in table 1 to aid in checking implementation of the theory.

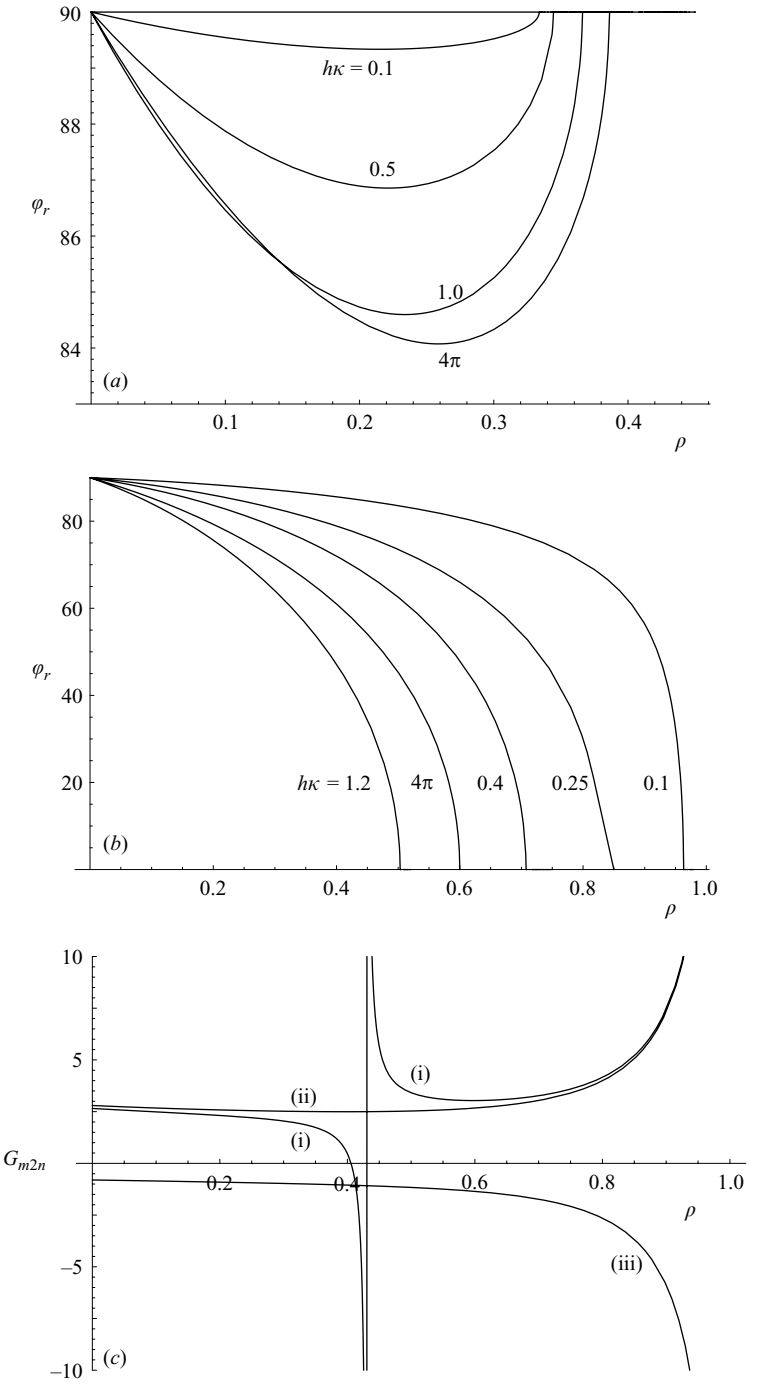


FIGURE 1. Identification and removal of singularities in the sub-harmonic transfer functions. (*a*) Roots $\varphi_r$ of (75) as function of $\rho$. (*b*) Roots $\varphi_r$ of (76) as function of $\rho$. (*c*) Sub- and super-harmonic transfer functions for the case of $\varphi = 40^\circ$ and $\kappa h = 1.2$. (i) $G^-_{m2n}$ (sub-harmonic); (ii) $\tilde{G}^-_{m2n}$ (filtered sub-harmonic); (iii) $G^+_{m2n}$ (super-harmonic).

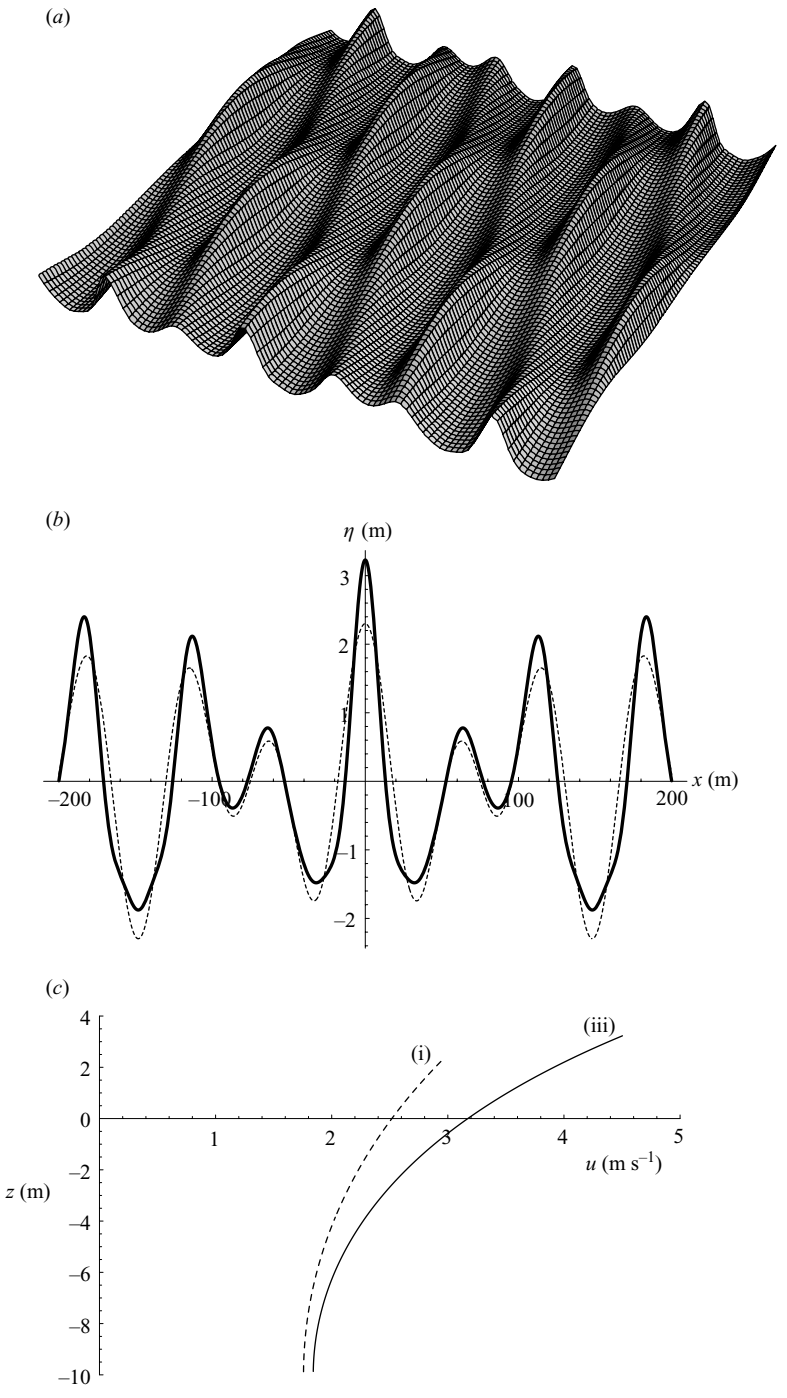


FIGURE 2. Third-order solution for a bichromatic short-crested wave in finite depth. Specifications: $h = 10\,\mathrm{m}$, $a_n = 1.3\,\mathrm{m}$, $a_m = 1.0\,\mathrm{m}$, $\omega_n = 2\pi \times 0.15\,\mathrm{s}^{-1}$, $\omega_m = 2\pi \times 0.10\,\mathrm{s}^{-1}$, $\varphi_n = 10^\circ$, $\varphi_m = -10^\circ$, $\boldsymbol{k}_n = \kappa_n(\cos\varphi_n, \sin\varphi_n)$, $\boldsymbol{k}_m = \kappa_m(\cos\varphi_m, \sin\varphi_m)$. (*a*) Perspective plot of the third-order surface elevation. (*b*) Surface elevation along the centreline (y = 0): first-order theory (dashed line); Third-order theory (full line). (*c*) Velocity profile at the centre point $(x, y) = (0,0)$: first-order theory (i); third-order theory (iii).

| Surface elevation | | Velocity potential | | Wavenumbers | |
|---|---|---|---|---|---|
| $\omega_{1n}$ | 0.9127 | $F_n$ | −6.5784 | $\kappa_n$ | 0.10737 |
| $\omega_{1m}$ | 0.6049 | $F_m$ | −13.2958 | $\kappa_m$ | 0.06514 |
| $G^-_{nm}$ | −1.4060 | $F^-_{nm}$ | 32.3669 | $\kappa^-_{nm}$ | 0.05125 |
| $G^+_{nm}$ | 3.1320 | $F^+_{nm}$ | −6.4505 | $\kappa^+_{nm}$ | 0.17004 |
| $G_{2n}$ | 2.5773 | $F_{2n}$ | −2.4552 | | |
| $G_{2m}$ | 4.6356 | $F_{2m}$ | −19.0648 | | |
| $G^-_{n2m}$ | −2.0753 | $F^-_{n2m}$ | −65.718 | $\kappa^-_{n2m}$ | 0.04703 |
| $G^+_{n2m}$ | 17.6333 | $F^+_{n2m}$ | −8.0446 | $\kappa^+_{n2m}$ | 0.23407 |
| $G^-_{m2n}$ | −4.8946 | $F^-_{m2n}$ | −14.8841 | $\kappa^-_{m2n}$ | 0.15513 |
| $G^+_{m2n}$ | 12.8636 | $F^+_{m2n}$ | −1.9582 | $\kappa^+_{m2n}$ | 0.27684 |
| $G_{3n}$ | 3.5572 | $F_{3n}$ | −0.1182 | | |
| $G_{3m}$ | 9.3713 | $F_{3m}$ | −10.705 | | |
| | | $F_{13n}$ | 0.1584 | | |
| | | $F_{13m}$ | 0.4267 | | |

TABLE 1. Third-order bichromatic short-crested wave in finite depth. Coefficients for the solution shown in figure 2.

## 4. The nonlinear dispersion relation for bichromatic interactions

### 4.1. *Generalization of the dispersion relation*

One of the key results of the new theory is the third-order amplitude dispersion for interacting bichromatic bi-directional waves in finite depth. This is given by (42) with $\omega_{3n}$ defined by (66). It is straightforward to generalize this result to more than two interacting waves, in which case we obtain

$$\omega_n = \boldsymbol{k}_n \cdot \boldsymbol{U} + \omega_{1n}\left(1 + c_n^2\kappa_n^2\left(\frac{8+\cosh 4h\kappa_n}{16\sinh^4 h\kappa_n}\right) + \sum_{m\neq n} c_m^2\kappa_m^2\Omega_{nm}\right), \tag{78}$$

where $\omega_{1n}$ is given by (19), $c_n$ and $c_m$ are defined by (17), and $\Omega_{nm}$ is given by (68)–(70). In the special case of zero net volume flux, the return current is determined by

$$\boldsymbol{U} = -\left(\frac{c_n^2\omega_{1n}}{2h\kappa_n}\coth h\kappa_n\right)\boldsymbol{k}_n - \sum_{m\neq n}\left(\frac{c_m^2\omega_{1m}}{2h\kappa_m}\coth h\kappa_m\right)\boldsymbol{k}_m. \tag{79}$$

These expressions, which are given in terms of the mean water depth $h$, allow for an assessment of the amplitude dispersion in several interacting waves, an issue which we will pursue in § 5 in connection with resonance conditions for finite-amplitude carrier waves and in § 6 in connection with nonlinear Bragg scattering.

Figure 3 shows the variation of the amplitude dispersion function $\Omega_{nm}$ as a function of $h\kappa_n$ and $h\kappa_m$ covering the range from shallow water to three times the conventional deep-water limit. Two different bichromatic interactions are considered: collinear interaction in figure 3($a$) and a short-crested interaction with wave angles $\varphi_n = 30^\circ$ and $\varphi_m = -30^\circ$ in figure 3($b$). In both cases, we notice that the largest values of $\Omega_{nm}$ (i.e. the largest influence on $\omega_n$) occur when $h\kappa_m < h\kappa_n$, i.e. longer waves have a stronger influence on shorter waves than vice versa.

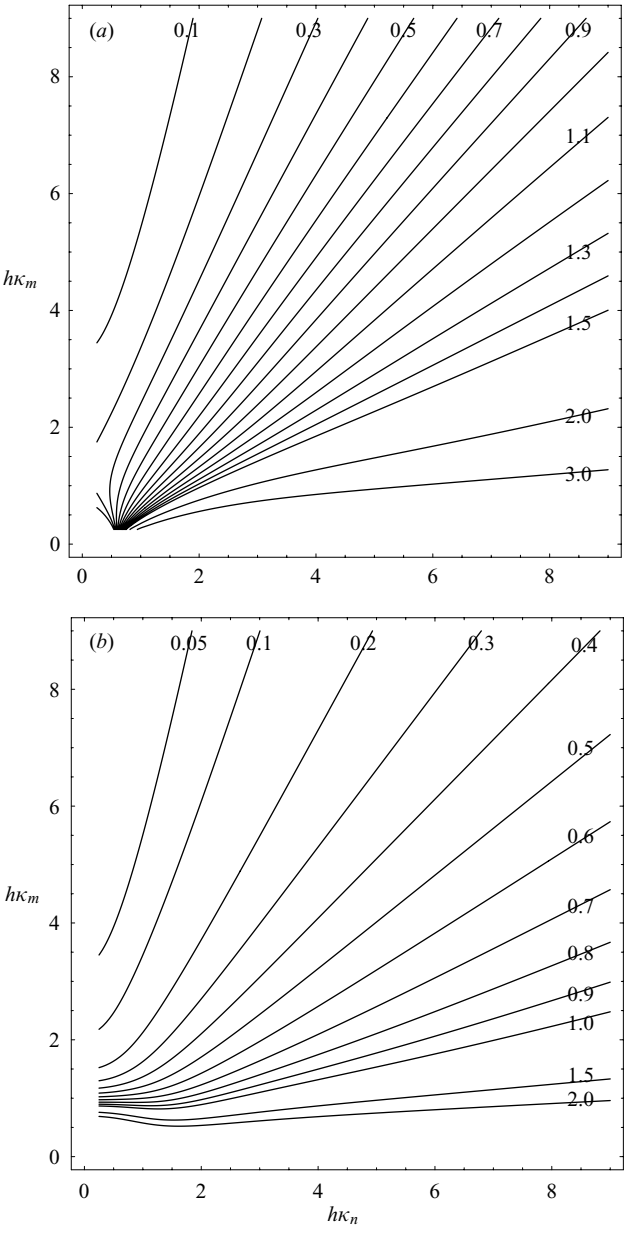


FIGURE 3. The amplitude dispersion function $\Omega_{nm}$ for bi-chromatic short-crested interactions as a function of wavenumbers $h\kappa_n$ and $h\kappa_m$. Definition of wavenumber vectors: $\boldsymbol{k}_n = \kappa_n(\cos\varphi_n, \sin\varphi_n)$, $\boldsymbol{k}_m = \kappa_m(\cos\varphi_m, \sin\varphi_m)$. (*a*) Collinear interaction, i.e. $\varphi_n = 0°$, $\varphi_m = 0°$. (*b*) Short-crested interaction with $\varphi_n = 30°$, $\varphi_m = -30°$.

### 4.2. *Bichromatic short-crested interactions in infinite depth*

Longuet-Higgins & Phillips (1962) were the first to calculate the change in phase speed of one train of gravity waves in the presence of another in infinite depth. A misprint in their solution was later corrected by Hogan *et al.* (1988), who extended

their solution to cover gravity-capillary waves in infinite depth. This extension was based on Zakharov's (1968) equation and it was given in terms of the Zakharov kernel $T(\boldsymbol{k}_1, \boldsymbol{k}_2, \boldsymbol{k}_3, \boldsymbol{k}_4)$. For gravity waves (no current) the solution by Hogan *et al.* can be expressed by

$$\omega_n = \omega_{1n}\left(1 + c_n^2\kappa_n^2\left(\frac{2\pi^2}{\kappa_n^3}T_{1111}\right) + c_m^2\kappa_m^2\left(\frac{4\pi^2\omega_{1m}}{\kappa_m^3\omega_{1n}}T_{1212}\right)\right), \tag{80}$$

where $T_{1111} \equiv T(\boldsymbol{k}_1, \boldsymbol{k}_1, \boldsymbol{k}_1, \boldsymbol{k}_1)$ and $T_{1212} \equiv T(\boldsymbol{k}_1, \boldsymbol{k}_2, \boldsymbol{k}_1, \boldsymbol{k}_2)$, while $\omega_{1n}$ and $\omega_{1m}$ here represent the infinite-depth limits of (19).

Unfortunately, it turns out that the determination of $T_{1111}$ and $T_{1212}$ requires a limiting process, where the identical wavenumber vectors must be perturbed slightly, i.e.

$$T_{1212} = \lim_{|\boldsymbol{\delta}_j|\to 0} T(\boldsymbol{k}_1 + \boldsymbol{\delta}_1, \boldsymbol{k}_2 + \boldsymbol{\delta}_2, \boldsymbol{k}_1 + \boldsymbol{\delta}_3, \boldsymbol{k}_2 + \boldsymbol{\delta}_4), \tag{81}$$

$$T_{1111} = \lim_{|\boldsymbol{\delta}_j|\to 0} T(\boldsymbol{k}_1 + \boldsymbol{\delta}_1, \boldsymbol{k}_1 + \boldsymbol{\delta}_2, \boldsymbol{k}_1 + \boldsymbol{\delta}_3, \boldsymbol{k}_1 + \boldsymbol{\delta}_4). \tag{82}$$

According to Janssen & Onorato (2005), the perturbation vectors should generally satisfy the resonance condition of the Zakharov equation, i.e.

$$\boldsymbol{\delta}_1 + \boldsymbol{\delta}_2 = \boldsymbol{\delta}_3 + \boldsymbol{\delta}_4. \tag{83}$$

In infinite depth, the outcome of the limiting process does not depend on the directions of the perturbation vectors (see e.g. Zakharov 1999), and the limit can be determined numerically or analytically. Zakharov (1999) gave an analytical result, which unfortunately includes some misprints. Hogan *et al.* (1988) found that (80) is in agreement with the corrected explicit expression by Longuet-Higgins & Phillips (1962).

For the case of collinear waves in infinite depth, (80) simplifies to

$$\omega_n = \sqrt{g\kappa_n}\left(1 + \tfrac{1}{2}c_n^2\kappa_n^2 + c_m^2\kappa_m^2\left(\frac{\kappa_n}{\kappa_m}\lambda\right)\right), \tag{84}$$

where

$$\lambda = \frac{\omega_{1n}}{\omega_{1m}} \quad \text{for } \kappa_m > \kappa_n, \qquad \lambda = \frac{\omega_{1m}}{\omega_{1n}} \quad \text{for } \kappa_m < \kappa_n.$$

This expression has been given by, for example, Zakharov (1999) and Zhang & Chen (1999).

We note that the self–self interaction term in (84) obviously agrees with the deep-water limit of the similar term in (78). We shall therefore concentrate on a comparison between the infinite-depth expression $\lambda\kappa_n/\kappa_m$ and the finite-depth expression defined by $\Omega_{nm}$. Figure 4 shows the percentage difference between the two in the deep-water regime as a function of $h\kappa_n$ and $h\kappa_m$ ranging from 3 to 9. We notice that discrepancies show up in a band along the diagonal, i.e. when $h\kappa_n$ and $h\kappa_m$ have similar magnitudes. The explanation is as follows. In the derivation of (84), it has been assumed that $\omega_{1n} \to \sqrt{g\kappa_n}$, $\omega_{1m} \to \sqrt{g\kappa_m}$ and that $\tanh(h(\kappa_n \pm \kappa_m)) \to 1$. This means that all interactions, including all possible sum and difference wavenumbers are assumed to take place in infinite depth. This assumption is generally not valid in practice, and explains why inaccuracies show up in a band along the diagonal in figure 4, where $\kappa_n$ and $\kappa_m$ are of similar magnitude. Surprisingly, this limitation in the infinite-depth theories of Longuet-Higgins & Phillips (1962), Hogan *et al.* (1988), Zakharov (1999) and Zhang & Chen (1999) has not previously been discussed, and in order to avoid

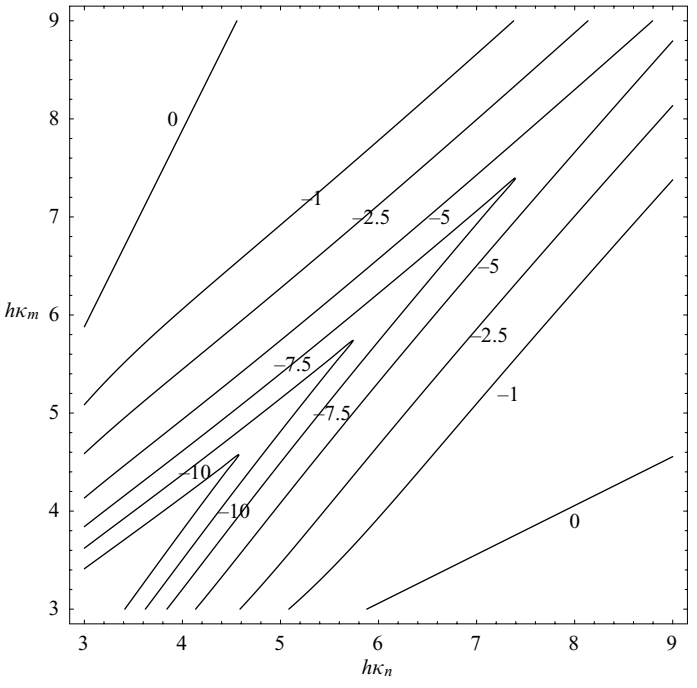


FIGURE 4. The percentage difference between $\Omega_{nm}$ defined by (68)–(70) for finite depth and $\lambda\kappa_n/\kappa_m$ defined by (84) for infinite depth. Collinear interactions.

potential inaccuracies, for example, in the description of irregular wavetrains, we recommend using the new finite-depth formulation under all circumstances.

### 4.3. *Bichromatic short-crested interactions in finite depth*

Finite-depth expressions for the Zakharov kernels $T(\boldsymbol{k}_1, \boldsymbol{k}_2, \boldsymbol{k}_3, \boldsymbol{k}_4)$ were given by, for example, Stiassnie & Shemer (1984); however, Agnon (1993), to our knowledge, was the first to consider the nonlinear dispersion relation in mutually interacting wavetrains in finite depth. His expression has the same form as (80), but with kernels modified to a finite depth. Unfortunately, he did not address the problem of evaluating $T_{1111}$ and $T_{1212}$ through the limiting process shown in (81)–(83), which is a non-trivial task. We have attempted to evaluate Agnon's expressions in finite depth, but have not been able to make these agree with (78). Apparently, the problem is that the Zakharov kernel function does not have a unique limit in finite depth, and the result depends on the direction of the perturbation vectors $\boldsymbol{\delta}_j$. So far only Janssen & Onorato (2005) have addressed this problem, and only for the case of monochromatic unidirectional waves in finite depth. The new theory provided in this paper may serve as a reference for future work on the application of Zakharov equations in finite depth.

### 4.4. *Monochromatic short-crested interactions*

When the frequencies and the amplitudes of the interacting wavetrains are identical, the present theory simplifies to the case of monochromatic short-crested waves. In this case, we may use $\omega_m = \omega_n$, $k_{mx} = k_{nx}$, $k_{my} = -k_{ny}$ and $a_m = a_n = a/2$, $b_m = b_n = 0$. With this choice, the first-order phase functions in (13) simplify to $\theta_n = (\omega_n t - k_{nx}x - k_{ny}y)$ and $\theta_m = (\omega_n t - k_{nx}x + k_{ny}y)$; the second-order phase functions in (24) simplify to $\theta_n + \theta_m = (2\omega_n t - 2k_{nx}x)$, $\theta_n - \theta_m = (2k_{ny}x)$, $2\theta_n = (2\omega_n t - 2k_{nx}x - 2k_{ny}y)$

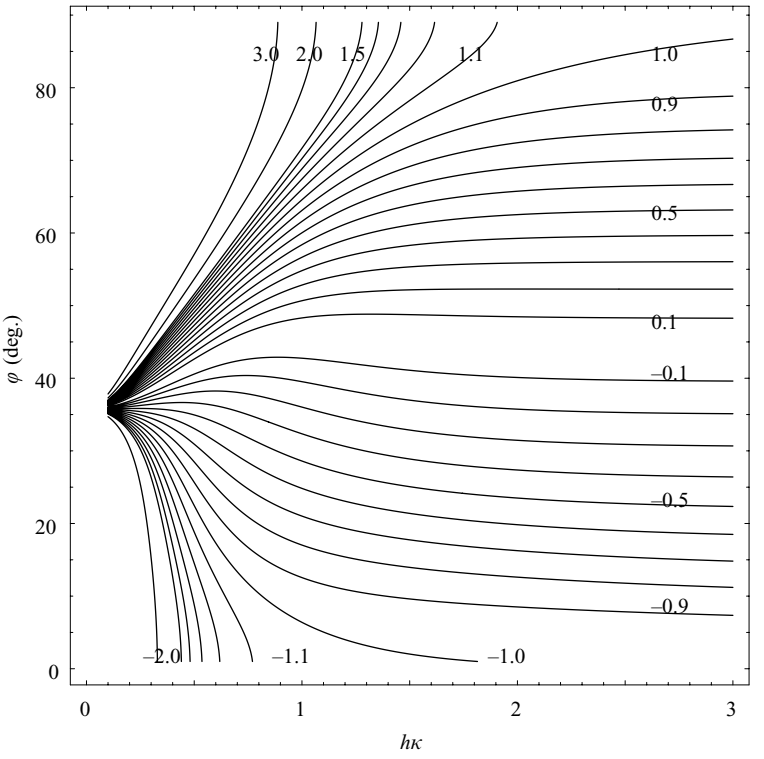


FIGURE 5. The amplitude dispersion function $\Omega_{nm}$ for monochromatic short-crested interactions as a function of wavenumber $h\kappa$ and wave angle $\varphi$. Definition of wavenumber vectors: $\boldsymbol{k}_n = \kappa(\sin\varphi, \cos\varphi)$, $\boldsymbol{k}_m = \kappa(\sin\varphi, -\cos\varphi)$.

and $2\theta_m = (2\omega_n t - 2k_{nx}x + 2k_{ny}y)$; while the third-order phase functions in (40) simplify to $\theta_n + 2\theta_m = (3\omega_n t - 3k_{nx}x + k_{ny}y)$, $\theta_n - 2\theta_m = (\omega_n t - k_{nx}x + 3k_{ny}y)$, $2\theta_n + \theta_m = (3\omega_n t - 3k_{nx}x - k_{ny}y)$, $2\theta_n - \theta_m = (\omega_n t - k_{nx}x - 3k_{ny}y)$, $3\theta_n = (3\omega_n t - 3k_{nx}x - 3k_{ny}y)$ and $3\theta_m = (3\omega_n t - 3k_{nx}x + 3k_{ny}y)$. It is straighforward to show that the present theory simplifies to the third-order solution by Hsu *et al.* (1979), except for the following discrepancy. While we have chosen to eliminate third-order secular terms by adding the $F_{13n}$-term to the velocity potential, Hsu *et al.* used an alternative, but equivalent, adjustment of the surface elevation (the $b_{11}$ term in their equation (58)). This is a free choice and both formulations are consistent steady third-order solutions.

The monochromatic short-crested case may conveniently be defined by the wavenumber vectors $\boldsymbol{k}_n = \kappa(\sin\varphi, \cos\varphi)$ and $\boldsymbol{k}_m = \kappa(\sin\varphi, -\cos\varphi)$. Now $\Omega_{nm}$ can be plotted as a function of $h\kappa$ and $\varphi$, as shown in figure 5 for $h\kappa$ ranging from shallow water to deep water. Note that for $\varphi > 45°$, the angle between the receiving wave and the interacting wave is less than 90° and in this case the interacting wave will have a component which is in the direction of the receiving wave. This results in a positive value of $\Omega_{nm}$. For $\varphi = 45°$, the two waves cross each other at right angles and consequently $\Omega_{nm} \to 0$. For $\varphi < 45°$, the interacting wave will have a component in the opposite direction of the receiving wave, which leads to negative values of $\Omega_{nm}$.

Roberts (1983) computed a twenty-seventh-order perturbation solution to monochromatic short-crested waves in infinite depth. A comparison with his solution makes it possible to quantify the applicability of the third-order theory to finite-amplitude

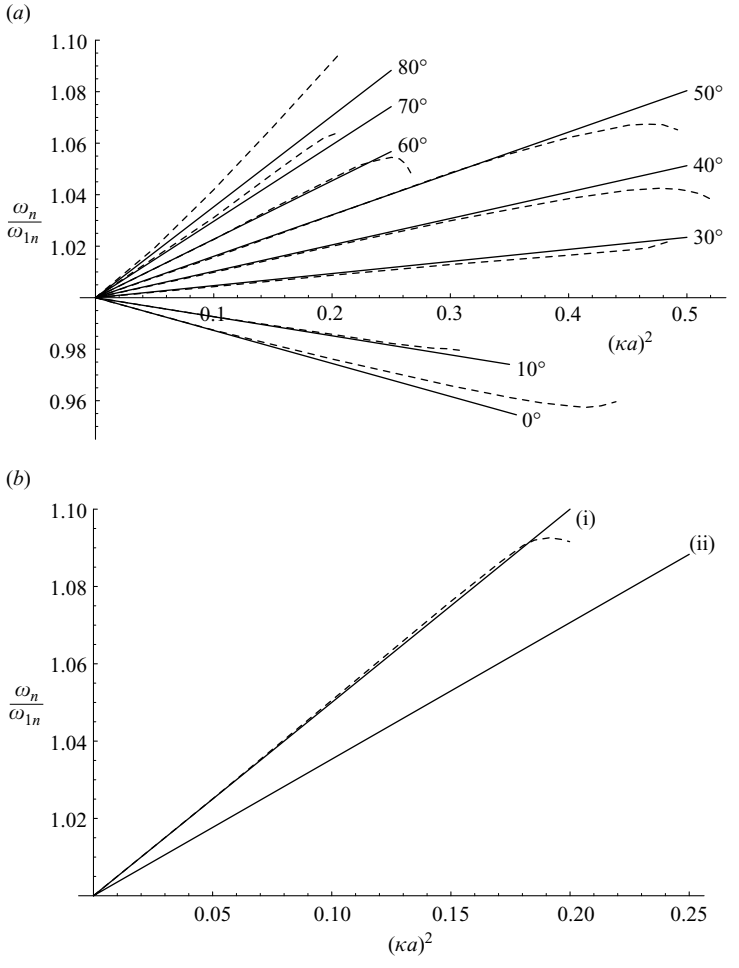


FIGURE 6. The nonlinear frequency of a short-crested wave as a function of the wave steepness squared. (*a*) Wave angles $\varphi$ covering the interval from 0° to 80°. Third-order theory is shown as full lines. Dashed lines are from the twenty-seventh-order solution by Roberts (1983), his figure 5. (*b*) The unidirectional case of $\varphi = 90°$. (i) Third-order theory for a single wave; (ii) the limit of third-order short-crested theory. Dashed line based on Cokelet (1977).

waves. Again we define the wavenumber vectors as shown above, i.e. $\varphi = 0°$ corresponds to purely standing waves and $\varphi = 90°$ corresponds to collinear progressive waves. We use $\boldsymbol{U} = 0$ and $c_n = c_m = a/2$, hence (78) simplifies to

$$\omega_n = \omega_{1n}\left(1 + \tfrac{1}{4}\kappa^2 a^2\left(\Omega_{nm} + \frac{8 + \cosh 4h\kappa}{16\sinh^4 h\kappa}\right)\right).$$

Figure 6(*a*) shows the relative nonlinear frequency $\omega_n/\omega_{1n}$ as a function of the wave steepness squared ($\kappa^2 a^2$) for a variety of angles $\varphi$. The third-order theory is shown as bold straight lines, while the high-order solution by Roberts (1983) is shown as dashed lines. For midrange values of $\varphi$, the surface elevation has a pyramidal shape, which is associated with relatively large maximum amplitudes, and in this range, the third-order theory is seen to be fairly accurate for $\kappa a$ as high as 0.6. Discrepancies

rapidly increase for $75^\circ < \varphi \leqslant 90^\circ$, in which case the surface shapes start to become long-crested.

Figure 6(*b*) shows $\omega_n/\omega_{1n}$ in the collinear limit of $\varphi = 90^\circ$. In this case the dashed line represents the solution by Cokelet (1977), while the third-order theory has been applied in two different ways: (i) accounting for the third-order single-wave theory for a progressive wave with steepness $\kappa a$, and in this case the agreement with Cokelet (1977) is extraordinarily good; (ii) accounting for the third-order short-crested solution, which consists of two identical components each with steepness $\kappa a/2$. Obviously, the short-crested solution does not converge towards the monochromatic single-wave solution for $\varphi \to 90^\circ$ and instead of a slope of $1/2\ \kappa^2 a^2$, it leads to a slope of $3/8\ \kappa^2 a^2$, significantly underestimating the effect of the amplitude dispersion. This problem of grazing angles was treated by Roberts & Peregrine (1983), who derived a special 'near-field' solution under the assumption that the derivatives in the direction along the crest (the $y$-direction) are small compared with those in the direction of propagation (the $x$-direction). As a consequence, the sinusoidal functions in the $y$-direction were replaced by Jacobian elliptic functions, and the resulting nonlinear frequency was expressed by

$$\omega_n = \omega_{1n}(1 + \kappa^2 a^2 \Omega_*), \qquad \Omega_* = \frac{1}{4}\left(1 + \frac{1}{m} - \frac{\pi^2}{4mK^2}\right),$$

with $K(m)$ being the complete elliptic integral of the first kind. In terms of nonlinear dispersion, this expression is able to bridge the gap between the unidirectional Stokes solution and the monochromatic short-crested solution as $\Omega_*$ approaches $1/2$ for $m \to 1$ and $3/8$ for $m \to 0$.

We emphasize that the general bichromatic short-crested solution does not have a similar problem with grazing angles. First of all, the nonlinear dispersion relation (78) has a continous transition from the grazing short-crested case to the collinear case (as long as the interacting frequencies are different). Secondly, the surface pattern in the grazing short-crested case is significantly more rounded for bichromatic waves than for monochromatic waves (see figure 2), which means that there is less need for a special treatment of $y$-derivatives versus $x$-derivatives. Thirdly, the bichromatic short-crested solution does not have a singularity at $\varphi = 90^\circ$, and therefore there will be no abrupt transition to the collinear case. As shown in figure 1($a$, $b$) singularities do appear, but at other angles, and they can be removed as discussed in § 3.5.

## 5. Resonance conditions for finite-amplitude carrier waves and their three-dimensional perturbations

In this section, we use the new third-order theory to evaluate the resonance conditions for the interaction of finite-amplitude waves and infinitesimal three-dimensional perturbations of arbitrary wavelength. In this connection, we shall demonstrate the importance of amplitude dispersion for the location of the resonance curves. The dominant instabilities can obviously not be detected by the present theory, and for this purpose we involve the stability method presented by McLean (1982).

McLean considered the stability of finite-amplitude unidirectional waves to three-dimensional perturbations. At first, he expressed the fully nonlinear governing equations in a frame of reference moving with the steady two-dimensional carrier wave. Next, the three-dimensional infinitesimal perturbations were superimposed on the steady wave, and the governing equations were linearized with respect to the perturbations with boundary conditions satisfied on the unperturbed free surface. For

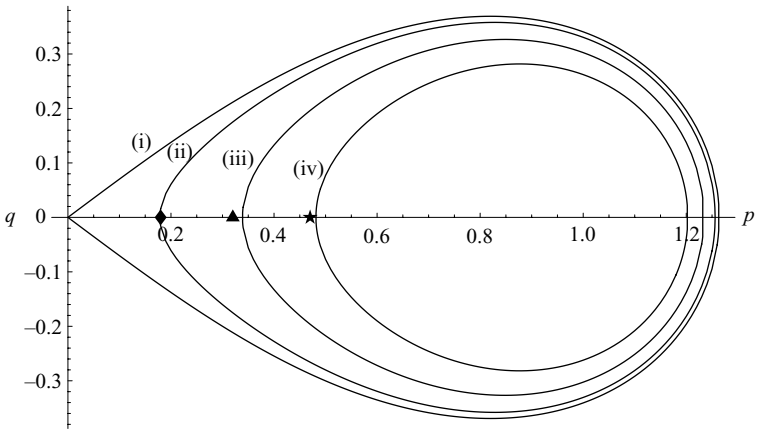


FIGURE 7. Resonance curves of class I for unidirectional carrier waves (i.e. $\varphi = 90°$). Third-order dispersion relation: (i) $\kappa a = 0.0$; (ii) $\kappa a = 0.1$; (iii) $\kappa a = 0.2$; (iv) $\kappa a = 0.3$. Points correspond to dominant instabilities from the method of McLean (1982): ◆, $\kappa a = 0.1$; ▲, $\kappa a = 0.2$; ★, $\kappa a = 0.3$.

a given set of wavenumber vectors, this procedure leads to an eigenvalue problem for the non-dimensional frequency ($\sigma$) of the perturbations, and instabilities correspond to $\mathrm{Im}\{\sigma\} > 0$. We have implemented this method in order to make additional examples which were not given by McLean.

McLean considered two types of instability, which are defined by the resonance conditions

$$\boldsymbol{k}_1 + \boldsymbol{k}_2 - 2\boldsymbol{k}_0 = 0, \qquad \omega_1 + \omega_2 - 2\omega_0 = 0, \qquad \text{class I}, \tag{85}$$

$$\boldsymbol{k}_1 + \boldsymbol{k}_2 - 3\boldsymbol{k}_0 = 0, \qquad \omega_1 + \omega_2 - 3\omega_0 = 0, \qquad \text{class II}, \tag{86}$$

where $\boldsymbol{k}_0$ represents the finite-amplitude carrier wave, while $\boldsymbol{k}_1$ and $\boldsymbol{k}_2$ represent the perturbations. With the choice of $\boldsymbol{k}_0 = (\kappa, 0)$, these conditions can be satisfied with perturbations described by

$$\boldsymbol{k}_1 = (1 + p, q)\kappa, \quad \boldsymbol{k}_2 = (1 - p, -q)\kappa, \qquad \text{class I}, \tag{87}$$

$$\boldsymbol{k}_1 = (1 + p, q)\kappa, \quad \boldsymbol{k}_2 = (2 - p, -q)\kappa, \qquad \text{class II}. \tag{88}$$

Note that $\omega_0$, $\omega_1$ and $\omega_2$ are the angular frequencies corresponding to the wavenumber vectors $\boldsymbol{k}_0$, $\boldsymbol{k}_1$ and $\boldsymbol{k}_2$. While it is common to assume that the frequencies involved in the resonance conditions satisfy the linear dispersion relation (see e.g. Phillips 1960; Longuet-Higgins & Phillips 1961; Hogan *et al.* 1988; Liu & Yue 1998), we emphasize that it is generally necessary to include amplitude dispersion in order to fully satisfy these conditions. As the perturbations are assumed to have infinitesimal wave heights, they cannot influence the angular frequency of the carrier wave $\omega_0$, which is only influenced by self–self interaction. In contrast, the angular frequencies of the perturbations $\omega_1$ and $\omega_2$ will be strongly influenced by the wave height of the carrier wave, while they will experience no self–self interaction. These effects can be estimated easily using (78) and as a result we can determine the $(p, q)$ values which satisfy the nonlinear frequency conditions in (85) and (86) for a given value of $\kappa a$, where $a$ is the amplitude of the carrier wave.

In the following examples, we consider the case of $\kappa h = 2\pi$. Figure 7 shows the class I resonance curves obtained by solving (85) for four different values of $\kappa a$. The

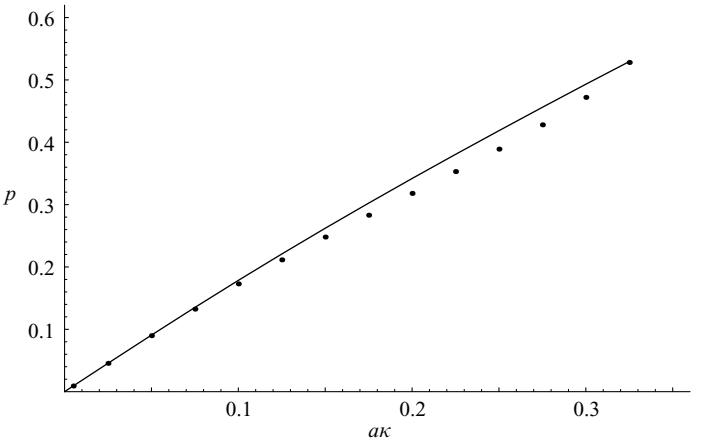


FIGURE 8. Third-order resonance curve of class I for unidirectional carrier waves (i.e. $\varphi = 90°$) with $q = 0$. Points correspond to dominant instabilities determined by the method of McLean (1982).

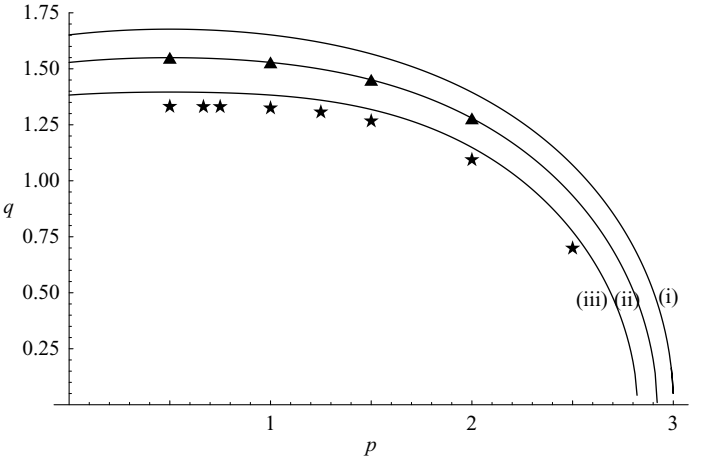


FIGURE 9. Resonance curves of class II for unidirectional carrier waves (i.e. $\varphi = 90°$). Third-order dispersion relation: (i) $\kappa a = 0.0$; (ii) $\kappa a = 0.2$; (iii) $\kappa a = 0.3$. Points correspond to dominant instabilities determined by the method of McLean (1982): ▲, $\kappa a = 0.2$; ★, $\kappa a = 0.3$.

nonlinearity obviously plays an important role in the location of these curves. By using the fully nonlinear method of McLean, we can determine the position of the dominant instabilities. They all occur for $q = 0$, and the points are seen to be close to the respective third-order resonance curves. A closer inspection of class I resonance with $q = 0$ is made in figure 8 which shows the variation of $p$ as a function of $\kappa a$. Again the third-order solution is in fairly good agreement with the McLean analysis, at least for $\kappa a < 0.15$. Figure 9 shows the class II resonance curves obtained by solving (86) for three different values of $\kappa a$. The data points obtained from the method of McLean are in close agreement with the third-order curves. A closer inspection of class II resonance with $p = 0.5$ is made in figure 10 which shows the variation of $q$ as a function of $\kappa a$. This leads to the so-called L2 crescent wave formations (see e.g.

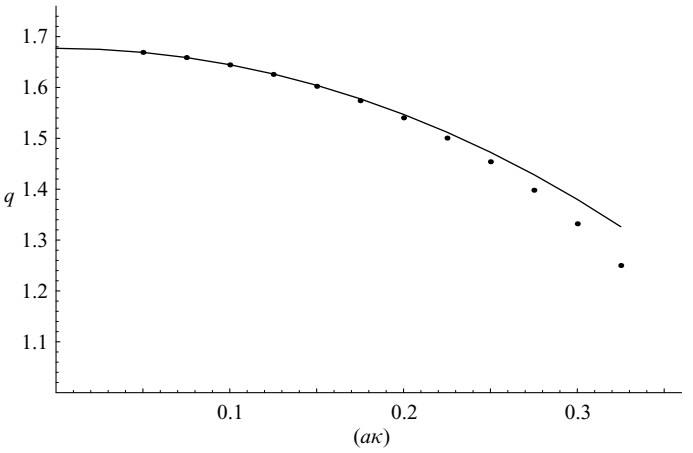


FIGURE 10. Third-order resonance curve of class II for unidirectional carrier waves (i.e. $\varphi = 90°$) with $p = 0.5$. Points correspond to dominant instabilities determined by the method of McLean (1982).

Fuhrman, Madsen & Bingham 2004), and again the agreement with the method of McLean is very good for $\kappa a < 0.25$.

## 6. Resonance conditions for Bragg scattering over an undular sea bed

Water waves travelling over an undular sea bottom are exposed to Bragg scattering, which typically results in partial reflection of the incoming wavetrain. The interaction of the surface waves and the bottom ripples is in many ways analogous to the mechanism of nonlinear wave–wave interaction for surface waves, and resonance conditions are obtained simply by adding the stationary bottom ripple wavenumbers to the resonance condition for the surface waves. Three different types of Bragg scattering have been discussed in the literature with resonance conditions given by

$$\boldsymbol{k}_1 \pm \boldsymbol{k}_2 \pm \boldsymbol{K} = 0, \qquad \omega_1 \pm \omega_2 = 0, \qquad \text{class I} \tag{89}$$

$$\boldsymbol{k}_1 \pm \boldsymbol{k}_2 \pm \boldsymbol{K}_1 \pm \boldsymbol{K}_2 = 0, \qquad \omega_1 \pm \omega_2 = 0, \qquad \text{class II} \tag{90}$$

$$\boldsymbol{k}_1 \pm \boldsymbol{k}_2 \pm \boldsymbol{k}_3 \pm \boldsymbol{K} = 0, \qquad \omega_1 \pm \omega_2 \pm \omega_3 = 0, \qquad \text{class III} \tag{91}$$

where $\boldsymbol{K}_j$ are the bottom wavenumber vectors, $\boldsymbol{k}_j$ are the surface wavenumber vectors and $\omega_j$ are the corresponding angular frequencies. Classes I and II have both been studied extensively in the literature and can both be treated by linear wave theory. In contrast, class III Bragg scattering involves nonlinear wave interaction and is a relatively new phenomenon, first discussed and analysed by Liu & Yue (1998). It defines a quartet interaction involving one ripple wavenumber vector $\boldsymbol{K}$ and three surface wavenumber vectors $\boldsymbol{k}_1$, $\boldsymbol{k}_2$ (both being incoming waves) and $\boldsymbol{k}_3$ (the scattered wave). As a special feature, the scatter arising from class III may result in either a reflected wave or a transmitted wave depending on the interacting wavenumbers.

In the following we shall concentrate on class III and apply the new third-order theory to determine the resonance curves. We consider normal incidence and assume that the two incoming waves are identical, i.e. $\boldsymbol{k}_2 = \boldsymbol{k}_1 = (\kappa_1, 0)$, $\boldsymbol{k}_3 = (\kappa_3, 0)$ and $\boldsymbol{K} = (K, 0)$. In this case, (91) leads to two possible resonance conditions

$$\kappa_3 = 2\kappa_1 - K, \qquad \omega_3 = 2\omega_1, \qquad \text{reflection (class III)}, \tag{92}$$

$$\kappa_3 = 2\kappa_1 + K, \qquad \omega_3 = 2\omega_1, \qquad \text{transmission (class III)}. \tag{93}$$

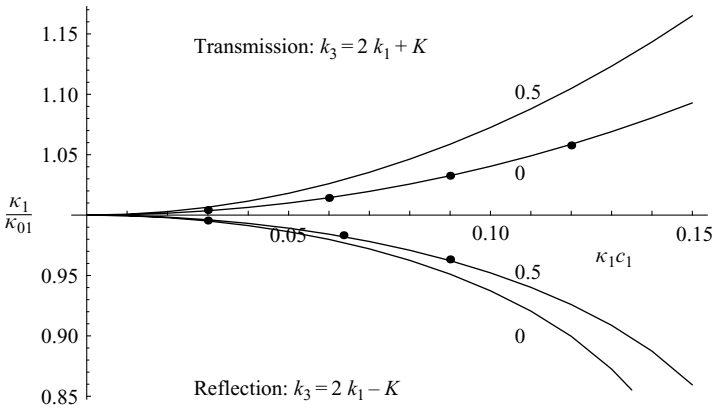


FIGURE 11. Downshift/upshift of the location of class III Bragg reflection/transmission as a function of incoming wave steepness $\kappa_1 c_1$. The shift is defined as the ratio of the nonlinear resonance wavenumber $\kappa_1$ to the linear resonance wavenumber $\kappa_{01}$. Specifications: $K = 2.642\,\mathrm{m}^{-1}$ and $h = 1.0\,\mathrm{m}$. ——, theoretical solutions for $c_3/c_1 = 0.0$ and $c_3/c_1 = 0.5$; ●, numerical results from Madsen *et al.* (2006).

In both cases, the scattered wave will occur at a frequency twice that of the incoming wave. In order to predict the location of the resonance, Liu & Yue invoked the linear dispersion relations

$$\omega_1 = \sqrt{g\kappa_1 \tanh \kappa_1 h}, \qquad \omega_3 = \sqrt{g\kappa_3 \tanh \kappa_3 h}, \tag{94}$$

which were solved in combination with (92)–(93) to determine $\kappa_1$ and $\kappa_3$ for given $h$ and $K$. As an example, they considered $K = 2.642\,\mathrm{m}^{-1}$ and $h = 1.0\,\mathrm{m}$, which leads to resonant reflection at $\kappa_3 = 0.546K$ for an incident wavenumber of $\kappa_1 = 0.227K$, and resonant transmission at $\kappa_3 = 2.195K$ for an incident wavenumber of $\kappa_1 = 0.598K$. While these estimates are valid for infinitesimal incoming waves, they become inaccurate for increasing nonlinearities. To improve this prediction, we replace (94) by (78) using $\boldsymbol{U} = 0$. The combination of (92)–(93) and (78) now leads to the determination of $\kappa_1$ and $\kappa_3$ for a given $h$, $K$, $c_1$ and $c_3$. Unfortunately, the amplitude $c_3$ of the scattered wave is unknown until actual Bragg scatter computations have been made, but typical values of $c_3/c_1$ fall in the interval from zero to 0.5 so these two extremes will be considered. Again we consider the case of $K = 2.642\,\mathrm{m}^{-1}$ and $h = 1.0\,\mathrm{m}$, and calculate the resonating $\kappa_1$ and $\kappa_3$ as a function of the incoming wave steepness $\kappa_1 c_1$.

The results are presented in figure 11 as the ratio $\kappa_1/\kappa_{01}$, where $\kappa_{01}$ is the result of applying the linear dispersion relations (94). With increasing nonlinearity we notice a clear upshift/downshift for the case of transmission/reflection. Actually, this trend can be seen in the numerical results by Liu & Yue (1998), although no explanation was given. Additional computations of class III Bragg scatter have recently been made by Madsen *et al.* (2006) and these results are included in figure 11. We notice that for the case of reflection, the numerical results follow the prediction corresponding to $c_3/c_1 = 0.5$, whereas for the case of transmission they follow the prediction corresponding to $c_3/c_1 = 0$. The explanation is the following. In the case of transmission, the incoming waves upstream of the ripple patch will not be influenced by the scattered wave until after the patch, hence the resonance over the patch will occur as if $\omega_1$ is not influenced by $c_3$ (i.e. as if $c_3$ is zero), while $\omega_3$ will be strongly

influenced by $c_1$. In the case of reflection, the incoming waves upstream of the patch will (at least eventually) be influenced by the reflected waves, and in this case $\omega_1$ and $\omega_3$ will both be influenced by mutual interactions corresponding to the actual wave amplitudes $c_1$ and $c_3$.

## 7. Concluding remarks

In this work, we have derived a new third-order perturbation solution for bi-directional bichromatic water waves in finite depth. The solution is an extension of Sharma & Dean (1981) from second-order to third-order, it is an extension of Hsu *et al.* (1979) from monochromatic to bichromatic short-crested waves, and it is an extension of Zhang & Chen (1999) from collinear interactions in infinite depth to bi-directional interactions in finite depth. The solution includes explicit expressions for the surface elevation and the vertical variation of the velocity potential, which is important for the determination of forces on sea walls and breakwaters. We also explicitly provide the velocity potential at the free surface (Appendix), which is useful for wavemaking in numerical models. Last but not least, the nonlinear dispersion relation is generalized to account for many interacting wave components with different frequencies and amplitudes. This allows for an easy assessment of the phase velocity of each of the wave components influenced by the presence of numerous others. All expressions unambiguously include the effect of an ambient current, with the option of specifying zero net volume flux.

The theory is derived and presented in §§ 3.1–3.3, while the resulting depth-averaged and time-averaged volume flux is determined in § 3.4. Section 3.5 includes the identification and removal of singularities in the third-order transfer functions. In contrast to the case of monochromatic short-crested waves, where singularities are located at the collinear limit, they can be found for any angle in the bichromatic case (see figure 1). A simple example of a bichromatic short-crested wave at a grazing angle is computed in § 3.6 (figure 2 and table 1). We emphasize that the surface shapes turn out to be much more rounded than the similar monochromatic case, and that there is no problem with the transition from the short-crested solution to the collinear solution as long as the frequencies are different. This is also in contrast to the monochromatic grazing angle case, which called for special treatment by Roberts & Peregrine (1983).

The nonlinear dispersion relation is discussed in detail in § 4. In § 4.1, we generalize the new expression to account for many interacting wave components with different frequencies and amplitudes, including the effect of a possible ambient current. Figure 3 shows the amplitude dispersion as a function of the interacting wavenumbers for collinear waves and for waves at an angle of $\pm 30^\circ$. In 4.2, we dicuss the infinite-depth expressions given by, for example, Longuet-Higgins & Phillips (1962), Hogan *et al.* (1988), Zakharov (1999) and Zhang & Chen (1999). We compare these expressions to our new finite-depth formulation and show that inaccuracies occur whenever the interacting wavenumbers are of similar magnitude (figure 4). The reason is that the infinite-depth approximations implicitly assume that, for example, $\tanh h(\kappa_n - \kappa_m) \to 1$, that is, that all interactions (including all possible difference-frequencies) take place in infinite depth. This assumption is generally not valid and in practice, this is a severe limitation of, for example, the third-order irregular infinite-depth theory by Zhang & Chen (1999). Instead, we recommend using the new finite-depth theory for all possible wave–wave interactions.

In § 4.3, we discuss the finite-depth Zakharov-type formulation by Agnon (1993). We have not been able to make this formulation agree with our new perturbation solution except at the deep-water limit. The reason is apparantly that the Zakharov kernel function does not have a unique limit in finite depth, and that the result depends on the direction of the infinitesimal vector in the limiting process. Janssen & Onorato (2005) have addressed this problem for monochromatic waves in finite depth, but so far the problem is unresolved for the more general case of bichromatic bi-directional waves. We expect that the new theory provided in this paper may serve as a reference for future work on the Zakharov formulation in finite depth.

In § 4.4, we discuss the case of monochromatic short-crested waves in finite and infinite depth. We show that in this case our theory simplifies to the theory of Hsu *et al.* (1979). The amplitude dispersion is shown as a function of wavenumber and wave angle in figure 5. The validity of the third-order theory is tested by comparing with the high-order infinite-depth solution by Roberts (1983) in figure 6.

In § 5, we demonstrate the usefulness of the nonlinear dispersion relation, by computing third-order resonance curves for unidirectional carrier waves and their three-dimensional infinitesimal perturbation satellites. The influence of nonlinearity on these curves is demonstrated and the curves are compared to the location of the dominant class I and class II wave instabilities determined by the numerical method of McLean (1982) in figures 7 to 10.

In § 6, we compute third-order resonance curves for class III Bragg scattering, which involves a nonlinear interaction between the incoming waves, the scattered waves and the sea bottom undulation. This, for the first time, explains the downshift/upshift of the resonating wavenumbers of the reflected/transmitted waves (figure 11), which was previously observed by Liu & Yue (1998).

This work has been financed by the Danish Technical Research Council (STVF Grant no. 9801635) and their support is greatly appreciated.

## Appendix. The velocity potential at the free surface

The third-order velocity potential at the free surface for bi-directional bichromatic waves is expressed as

$$
\begin{aligned}
\widetilde{\Phi} = {} & \boldsymbol{U}\cdot\boldsymbol{x} + \mu_n(a_n\sin\theta_n - b_n\cos\theta_n) + \mu_m(a_m\sin\theta_m - b_m\cos\theta_m)\\
& + \mu_{2n}(A_{2n}\sin 2\theta_n - B_{2n}\cos 2\theta_n) + \mu_{2m}(A_{2m}\sin 2\theta_m - B_{2m}\cos 2\theta_m)\\
& + \mu^+_{nm}(A^+_{nm}\sin(\theta_n+\theta_m) - B^+_{nm}\cos(\theta_n+\theta_m))\\
& + \mu^-_{nm}(A^-_{nm}\sin(\theta_n-\theta_m) - B^-_{nm}\cos(\theta_n-\theta_m))\\
& + \mu_{3n}(A_{3n}\sin 3\theta_n - B_{3n}\cos 3\theta_n) + \mu_{3m}(A_{3m}\sin 3\theta_m - B_{3m}\cos 3\theta_m)\\
& + \mu_{13n}(a_n\sin\theta_n - b_n\cos\theta_n) + \mu_{13m}(a_m\sin\theta_m - b_m\cos\theta_m)\\
& + \mu^+_{n2m}(A^+_{n2m}\sin(\theta_n+2\theta_m) - B^+_{n2m}\cos(\theta_n+2\theta_m))\\
& + \mu^-_{n2m}(A^-_{n2m}\sin(\theta_n-2\theta_m) - B^-_{n2m}\cos(\theta_n-2\theta_m))\\
& + \mu^+_{m2n}(A^+_{m2n}\sin(\theta_m+2\theta_n) - B^+_{m2n}\cos(\theta_m+2\theta_n))\\
& + \mu^-_{m2n}(A^-_{m2n}\sin(\theta_m-2\theta_n) - B^-_{m2n}\cos(\theta_m-2\theta_n)),
\end{aligned}
$$

where

$$\mu_n = -\frac{\omega_{1n}\coth h\kappa_n}{\kappa_n}, \qquad \mu_m = -\frac{\omega_{1m}\coth h\kappa_m}{\kappa_m},$$

$$\mu^{\pm}_{nm} = F^{\pm}_{nm}\cosh h\kappa^{\pm}_{nm} - \tfrac{1}{2}h(\omega_{1n} \pm \omega_{1m}),$$

$$\mu_{2n} = -\tfrac{1}{4}h\omega_{1n}\left(4 + \frac{3\cosh 2h\kappa_n}{\sinh^4 h\kappa_n}\right), \quad \mu_{2m} = -\tfrac{1}{4}h\omega_{1m}\left(4 + \frac{3\cosh 2h\kappa_m}{\sinh^4 h\kappa_m}\right),$$

$$\mu_{3n} = -\frac{h^2\kappa_n\omega_{1n}\coth h\kappa_n}{128\sinh^6 h\kappa_n}(26 - 3\cosh 2h\kappa_n + 10\cosh 4h\kappa_n + 3\cosh 6h\kappa_n),$$

$$\mu_{3m} = -\frac{h^2\kappa_m\omega_{1m}\coth h\kappa_m}{128\sinh^6 h\kappa_m}(26 - 3\cosh 2h\kappa_m + 10\cosh 4h\kappa_m + 3\cosh 6h\kappa_m),$$

$$\mu_{13n} = \frac{c_m^2}{2h}(F^+_{nm}\kappa^+_{nm}\sinh h\kappa^+_{nm} + F^-_{nm}\kappa^-_{nm}\sinh h\kappa^-_{nm} + \omega_{1m}(G^+_{nm} - G^-_{nm}))$$
$$+ F_{13n}\cosh h\kappa_n + \frac{\kappa_n\omega_{1n}\coth h\kappa_n}{16}\left(c_n^2\left(1 + \coth^2 h\kappa_n - \frac{7}{\sinh^2 h\kappa_n}\right) - 4c_m^2\right),$$

$$\mu_{13m} = \frac{c_n^2}{2h}(F^+_{mn}\kappa^+_{mn}\sinh h\kappa^+_{mn} + F^-_{mn}\kappa^-_{mn}\sinh h\kappa^-_{mn} + \omega_{1n}(G^+_{mn} - G^-_{mn}))$$
$$+ F_{13m}\cosh h\kappa_m + \frac{\kappa_m\omega_{1m}\coth h\kappa_m}{16}\left(c_m^2\left(1 + \coth^2 h\kappa_m - \frac{7}{\sinh^2 h\kappa_m}\right) - 4c_n^2\right),$$

$$\mu^{\pm}_{n2m} = -\frac{h^2\kappa_n\omega_{1n}\coth h\kappa_n}{4} + \frac{h^2\kappa_m\coth h\kappa_m}{4\sinh^2 h\kappa_m}(\mp 5\omega_{1m} - 2\omega_{1n} - (\omega_{1n} \pm \omega_{1m})\cosh 2h\kappa_m)$$
$$+ h(F^{\pm}_{nm}\kappa^{\pm}_{nm}\sinh h\kappa^{\pm}_{nm} \mp \omega_{1m}G^{\pm}_{nm}) + F^{\pm}_{n2m}\cosh h\kappa^{\pm}_{n2m},$$

$$\mu^{\pm}_{m2n} = -\frac{h^2\kappa_m\omega_{1m}\coth h\kappa_m}{4} + \frac{h^2\kappa_n\coth h\kappa_n}{4\sinh^2 h\kappa_n}(\mp 5\omega_{1n} - 2\omega_{1m} - (\omega_{1m} \pm \omega_{1n})\cosh 2h\kappa_n)$$
$$+ h(F^{\pm}_{mn}\kappa^{\pm}_{mn}\sinh h\kappa^{\pm}_{mn} \mp \omega_{1n}G^{\pm}_{mn}) + F^{\pm}_{m2n}\cosh h\kappa^{\pm}_{m2n}.$$

## REFERENCES


Agnon, Y. 1993 On a uniformly valid model for surface wave interaction. *J. Fluid Mech.* **247**, 589–601.

Bryant, P. J. 1985 Doubly periodic progressive permanent waves in deep water. *J. Fluid Mech.* **161**, 27–42.

Chappelear, J. E. 1961 On the description of short-crested waves. *Beach Erosion Board, US Army Corps Engrs.* TM 125.

Cokelet, E. D. 1977 Steep gravity waves in water of arbitrary uniform depth. *Phil. Trans. R. Soc. Lond.* A **286**, 183–230.

Fuchs, R. A. 1952 On the theory of short-crested oscillatory waves. *Gravity Waves, US Natl Bur. Stand. Circular* **521**, 187–200.

Fuhrman, D. R., Madsen, P. A. & Bingham, H. B. 2004 A numerical study of crescent waves. *J. Fluid Mech.* **513**, 309–341.

Hammack, J. L., Henderson, D. M. & Segur, H. 2005 Progressive waves with persistent two-dimensional surface patterns in deep water. *J. Fluid Mech.* **532**, 1–51.

Hammack, J. L., Scheffner, N. & Segur, H. 1989 Two-dimensional periodic waves in shallow water. *J. Fluid Mech.* **209**, 567–589.

Hogan, S. J., Gruman, I. & Stiassnie, M. 1988 On the changes in phase speed of one train of water waves in the presence of another. *J. Fluid Mech.* **192**, 97–114.

Hsu, J. R. C., Tsuchiya, Y. & Silvester, R. 1979 Third-order approximation to short-crested waves. *J. Fluid Mech.* **90**, 179–196.

Janssen, P. A. E. M. & Onorato, M. 2005 The shallow water limit of the Zakharov equation and consequences for (freak) wave prediction. *TM* 464. European Centre for Medium-Range Weather Forecasts (ECMWF), Reading, UK.

Kimmoun, O., Ioualalen, M. & Kharif, C. 1999 Instabilities of steep short-crested surface waves in deep water. *Phys. of Fluids* **11**, 1679–1681.

Krasitskii, V. P. 1994 On reduced equations in the Hamiltonian theory of weakly nonlinear surface waves. *J. Fluid Mech.* **272**, 1–20.

Liu, Y. & Yue, D. K. P. 1998 On generalized Bragg scattering of surface waves by bottom ripples. *J. Fluid Mech.* **356**, 297–326.

Longuet-Higgins, M. S. & Phillips, O. M. 1962 Phase velocity effects in tertiary wave interactions. *J. Fluid Mech.* **12**, 333–336.

McLean, J. W. 1982 Instabilities of finite-amplitude gravity waves on water of finite depth. *J. Fluid Mech.* **114**, 331–341.

Madsen, P. A., Fuhrman, D. R. & Wang, B. 2006 A Boussinesq-type method for fully nonlinear waves interacting with a rapidly varying bathymetry. *Coastal Engng* **53**, 487–504.

Phillips, O. M. 1960 On the dynamics of unsteady gravity waves of finite amplitude. Part 1. The elementary interactions. *J. Fluid Mech.* **9**, 193–217.

Pierson, W. J. Jr. 1993 Oscillatory third-order perturbation solutions for sums of interacting long-crested Stokes waves on deep water. *J. Ship Res.* **37**, 354–383.

Roberts, A. J. 1983 Highly nonlinear short-crested water waves. *J. Fluid Mech.* **135**, 301–321.

Roberts, A. J. & Peregrine, D. H. 1983 Notes on long-crested water waves. *J. Fluid Mech.* **135**, 323–335.

Roberts, A. J. & Schwartz, L. W. 1983 The calculation of nonlinear short-crested gravity waves. *Phys. Fluids* **26**, 2388–2392.

Schäffer, H. A. 1996 Second-order wavemaker theory for irregular waves. *Ocean Engng* **23**, 47–88.

Schäffer, H. A. & Steenberg, C. M. 2003 Second-order wavemaker theory for multidirectional waves. *Ocean Engng* **30**, 1203–1231.

Sharma, J. & Dean, R. 1981 Second-order directional seas and associated wave forces. *Soc. Pet. Engrs J.* 129–140.

Stiassnie, M. & Shemer, L. 1984 On modifications of the Zakharov equation for surface gravity waves. *J. Fluid Mech.* **143**, 47–67.

Zakharov, V. 1968 Stability of periodic waves of finite amplitude on the surface of a deep fluid. *J. Appl. Mech. Tech. Phys.(Engl. Transl.)* **9**, 190–194.

Zakharov, V. 1999 Statistical theory of gravity and capilary waves on the surface of a finite depth fluid. *Eur. J. Mech.* B/*Fluids* **18**, 327–344.

Zhang, J. & Chen, L. 1999 General third-order solutions for irregular waves in deep water. *J. Engng Mech.* **125**, 768–779.